GeoScienceWorld
Lithosphere
Volume 2021, Article ID 8876012, 23 pages
https://doi.org/10.2113/2021/8876012

Lithosphere

Research Article

Complete Strain Record of a Highly Asymmetric Shear Zone: From Fault Core Gouges to Surface Rupture of Historical Earthquakes in the Alhama de Murcia Fault (SE Iberian Peninsula)

J. Alonso-Henar,[1] **E. Rodríguez-Escudero**,[1] **P. Herrero-Barbero**,[1] **M. Tsige**,[1] **and J. J. Martínez-Díaz**[1,2]

[1]*Geodynamics, Stratigraphy and Paleontology Department, Geological Sciences Faculty, Complutense University of Madrid, 28040 Madrid, Spain*
[2]*Instituto de Geociencias IGEO (UCM-CSIC), 28040 Madrid, Spain*

Correspondence should be addressed to J. Alonso-Henar; jahenar@geo.ucm.es

Received 30 September 2020; Accepted 24 March 2021; Published 14 May 2021

Academic Editor: Andrea Billi

Classical models of fault rock architecture point to a relatively simple and symmetric architecture of a fault zone, where the fault core is a narrow foliated cataclasite (few centimeters) bounded by a thick damage zone developed cutting through host rocks. Those models are far from the studied fault rocks developed in the Alhama de Murcia Fault (AMF), SE Spain, where fault core is in contact with an almost no deformed hosting rock at one side and to a wide damage zone towards the opposite boundary. The AMF is an active shear zone and the source of destructive recent and historical earthquakes. It has more than 10 km accumulated slip, and it develops a more than 100 meters wide shear zone with fault rocks that have been continuously sampled and analyzed combining a drill core from a 174 m deep vertical borehole, six trenches excavation, and outcrop surfaces cleaning. Hand specimen and microanalyses were used to classify the fault rock in deformation domains in a strongly heterogeneous shear zone according to its lithologies and structural features. It ranges from 10 to 30 meters wide fault core, where steady strain occurs, to an intensely deformed damage zone where strain is concentrated along discrete gouge bands. Trenching also showed a surface rupture that offsets Arabic archaeological remains related to the 1674 catastrophic event occurred in Lorca (Murcia). Steady homogeneous deformation was found in the areas closest to the hanging wall, in the fault core, where Lower Paleozoic Schists are the potolith of ultrafault gouges. As deformation increased, the shear zone involved Permian-Triasic basement rocks and Miocene sedimentary rocks in heterogeneous deformation domains. In the lower domains, strain is located in anastomosing shear bands which are spatially related with a surface seismic rupture of the 1674 destructive earthquake.

1. Introduction

During the last decades, the study of fault rocks has increased and, thanks to the deep drilling of active faults, greatly advanced our understanding of fundamental processes of fault rock formation, their evolution, and influence in earthquake physics (e.g., [1–5]). Fault rocks take priority in the study of seismic processes, and their architecture and lithologies are key parameters in order to shed light on how kinematics and mechanics are spatially and temporally distributed in active shear zones (e.g., [6–10]). The fault zone architecture traditionally has been divided into three elements that compose a fault zone: the fault core, the damage zone, and the protolith. Caine et al. [11] considered that the "fault core is defined as the structural, lithologic and morphologic portion of a fault zone where most of the displacement is accommodated […]. A damage zone is the network of subsidiary structures that bound the fault core […] and [damage zone and fault core are surrounding by] a relatively undeformed protolith, the hosting rock". This model points to a relatively simple and symmetric architecture of a fault zone developed cutting through predominantly quartzofeldspathic host rocks, where the fault core is a relatively narrow foliated cataclasite (few centimeters) bounded by a thick

damage zone ([12]; Chester et al. 1993; [10, 11, 13]). When a fault is developed in a relatively phyllosilicate-rich hosting rock where strain harden may occur, Faulkner et al. [7], based on Carboneras Fault (SE Spain, and close to the study area Figure 1), realized that several strands of phyllosilicate-rich fault gouges appear (less than 5 m thick and considered to be the fault core) that bound lenses of variably deformed protolith. At these cases, the fault core cannot be considered as a simple, narrow, and prominent slip surface. For these reasons, in this study, and based on [12]; Chester et al., 1993; Bruhn et al., 1994; [11]; Clausen, 2002; Clausen et al., 2003, [7], we consider that (1) the fault core represents the part of the fault zone where most of the displacement is accommodated. It is in a steady step of the deformation (flow pattern and flow parameter remain constant during deformation) and consists of slip surfaces, fault gouges, some breccias, cataclasites, and geochemically altered rock bodies; (2) the damage zone is a deformed rock volume that limits with the fault core; it is in a nonsteady phase of deformation and is composed of subsidiary faults, fault rocks, and breccia; and (3) the hosting rock is a relatively undeformed protolith. Also, in this study, we have introduced the term Subsidiary Slip Zone (SSZ) in order to name gouge strands with more accommodated slip compared to the surrounding fault rocks, but that are not necessary part of the fault core. This term should not be confused with the term Principal Slip Zones that is used to describe one or more gouge or cataclasite strands within a fault core lithologically and structurally heterogeneous that accommodates most of the displacement along them (e.g., [14, 15]).

The Alhama de Murcia Fault (AMF) is an oblique left lateral strike-slip fault with reverse component located in the Eastern Betics (southeastern Spain, Figure 1), one of the areas with the greatest seismic and tectonic activity in the Iberian Peninsula (e.g., [16–19], Martínez-Diaz et al. 2012). In the central section of the AMF a >100 m thick fault (shear) zone that dips 55-70° to the NW appears showing a stacking of different domains composed of rocks from Lower Paleozoic to Quaternary [20]. The quality and quantity of its outcrops offer a good opportunity to get a complete record of the tectonic activity of this fault and understand how an inclined shear zone grows and distributes the strain. The AMF fault rock core has been studied for decades; mechanical or kinematic models have been proposed by, for example, Hall [21], Rutter et al. [20, 22], Niejemejer and Vissers [23], Rodriguez-Escudero et al. [24], or Alonso-Henar et al. [25]. Besides, there is an exceptional track of neotectonic and paleoseismological studies of the most recent strain increments in the Alhama de Murcia Fault that assign its seismic activity in several segments that helps to understand how strain is distributed in this fault zone (e.g., [18, 26–30], among others).

The aim of this study is to shed light on the influence that the fault zone lithologies and their distribution and architecture may have in the seismic behavior and the evolution at the medium and long terms of a fault zone. We have done a broad scale approach, from scanning electron microscope to cartographic scale, to the fault zone architecture and the analysis of the lithologies of more than 100 m wide fault rock. Combining 3D observations from trenches, drilling, and microanalyses, we have classified the fault rock in deformation domains. The existing architecture models do not satisfy the observations, and we propose an asymmetric strain model for this inclined shear zone, where the more intense and steady deformation is located in a boundary (fault core) and decreases gradually towards the opposite border (damage zone, where surface rupture of historical earthquakes occur).

2. Tectonic and Geological Setting

The Eastern Betic Shear Zone (EBSZ) forms the continuation towards the Northeast of the Trans Alboran Shear Zone [31, 32]. It is formed by a series of left lateral, oblique faults, with a reverse component, that extend about 250 km from Alicante to Almería: Bajo Segura, Carrascoy, Los Tollos, Alhama de Murcia, Palomares, and Carboneras faults (Sanz de Galdeano, 1990; [33–37]). The EBSZ faults accommodate much of the shortening during the Neogene-Quaternary (Sanz de Galdeano, 1990). The neotectonic transpressive period began at the end of the Neogene due to the Africa-Eurasia convergence, with a N150°E regional direction and rates of 5-6 mm/yr (Serpelloni et al., 2007; [38, 39]). The AMF is one of the largest faults of the Eastern Betics Shear Zone (Montenat, 1973, [37]), it has more than 10 km accumulated slip [20], and it is the source of Mw >6.5 historical and prehistorical earthquakes (Martinez-Diaz et al., 2001) and the source of the Lorca 2011 Mw 5.2 destructive earthquake [40]. The horizontal geodetic slip-rate of the AMF is 1.5 ± 0.3 mm/yr [39], and studies based on geologically measured indicators yielded a slip-rate of 1 ± 0.2 mm/yr in the central segments [41], which are considered high slip rates compared to the approximately 5 mm/year convergence between Nubia and Eurasian plates.

Martínez-Díaz et al. [42] divided the AMF into four seismogenic/structural segments: Goñar-Lorca segment (where this study is focused); Lorca-Totana segment, with an intense registered instrumental seismicity and several branches; Totana-Alhama de Murcia segment, with deformation distributed in several branches; and Alhama de Murcia-Alcantarilla segment, with a continuous trace but with less morphological expression ([27], Figure 1). Fault rocks associated with the AMF are well exposed in several outcrops along the Goñar-Lorca and Lorca-Totana segments. In the latter, the zone of active deformation consists of two branches, the main, northern branch had extruded the fault gouge, and a southern branch, where most of the studies on active tectonics were focused (e.g., [26]), and that until recently was the only branch considered active (the 2011 Lorca earthquake and the 1674 historical event had been recently assigned to this branch, e.g., [29, 42]). The present study is focused on the northeastern area of the Goñar-Lorca segment, which has the best record of fault rocks, and the strain is accommodated in a unique branch, where Martinez-Diaz et al. [29] identified the surface rupture of at least one historical earthquake. The fault rock is >100 m wide and developed across Paleozoic, Mesozoic, and Miocene rocks. Fault rock fabric

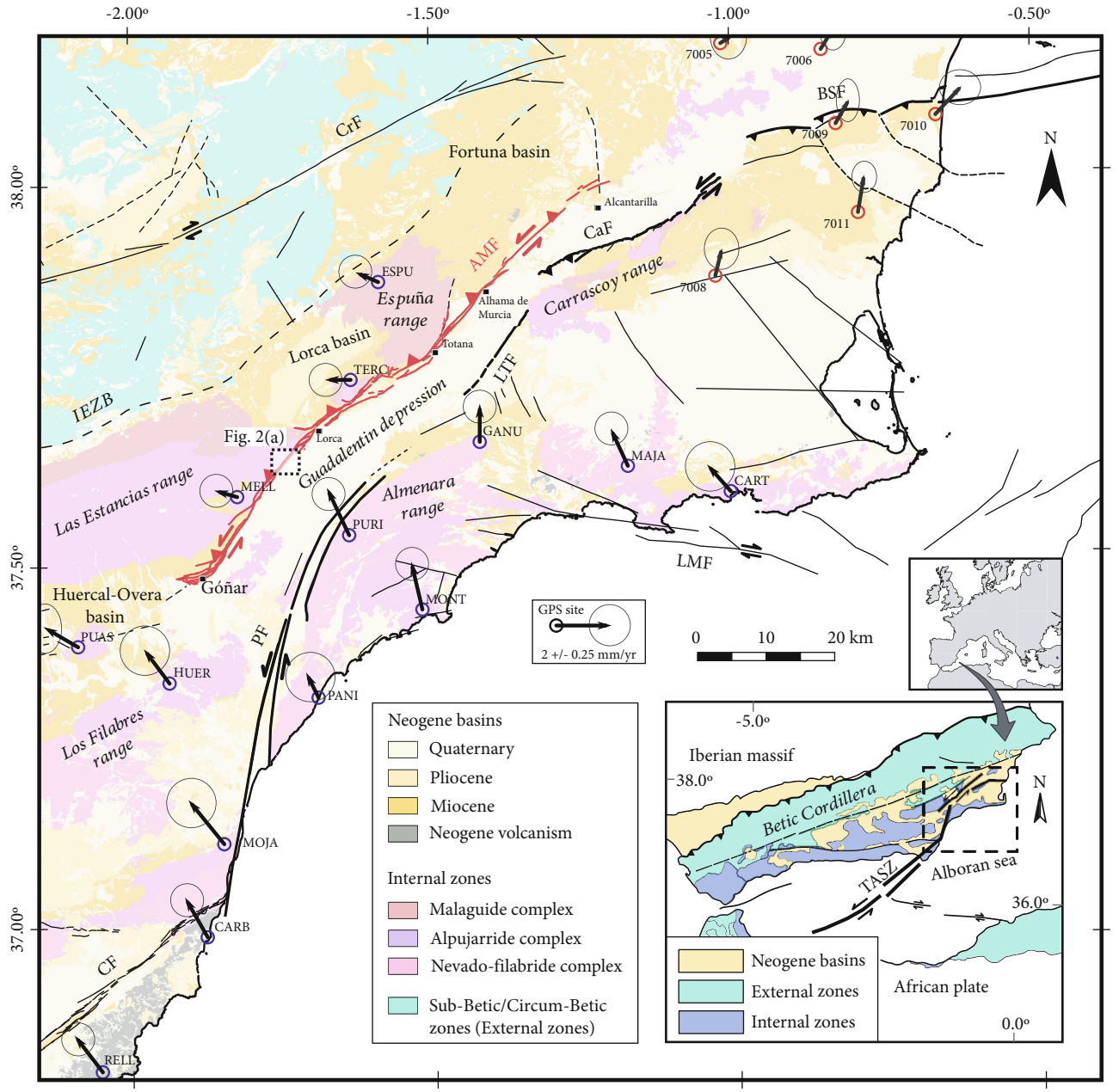

FIGURE 1: Geological sketch map of the surrounding area of the Alhama de Murcia fault (red line), showing the main structural units of the Eastern Betic Cordillera. The principal structures represented in the map are AMF: Alhama de Murcia Fault; CF: Carboneras Fault; PF: Palomares Fault; LTF: Los Tollos Fault; CaF: Carrascoy Fault; BSF: Bajo Segura Fault; CrF: Crevillente Fault; LMF: Las Moreras Fault; IEZB: Internal-External Zone Boundary (dashed line). The lower right inset shows the regional geological framework at the SE of Iberian Peninsula and the location of the Trans-Alboran Shear Zone (TASZ). The arrows represent the CuaTeNeo GPS network (with blue circles; [39]) and Bajo Segura GPS network (with red circles; [38]) in Eurasia-fixed reference frame.

is consistent with current geodynamics with no evidence of inherited previous fabrics (e.g., [20, 23, 43]).

The AMF is located in the Internal zone of the Betic cordlillera (Figure 1). The basement rocks of the study area are formed (from bottom to top) by the Nevado-Filábride complex, which represent the Variscan basement relicts made by Paleozoic and Triassic rocks [44], that are not observed in the AMF zone, and the Malaguide and Alpujárride tectonic complexes from the Alboran Domain [45]. The latter are the main protolith source for our fault rock. Basement rocks are overlain by Neogene sediments related to Burdigalian-Tortonian basins and Quaternary Alluvial deposits ([46]; Martínez-Martínez and Azañón 1997; [47], Figures 1 and 2). The Alpujarride Complex is made of (a) Lower Paleozoic Graphite Mica-Schists that locally could include greywackes [48–52]; (b) Permo-Triasic Fine Grained Blue/Gray Phyllites/Schists [53, 54]; and (c) Triassic Carbonates [55, 56]. The Malaguide Complex in the area is mostly made of Permo-Triassic wine red shales, sandstones, and conglomerates but some Upper Malaguide

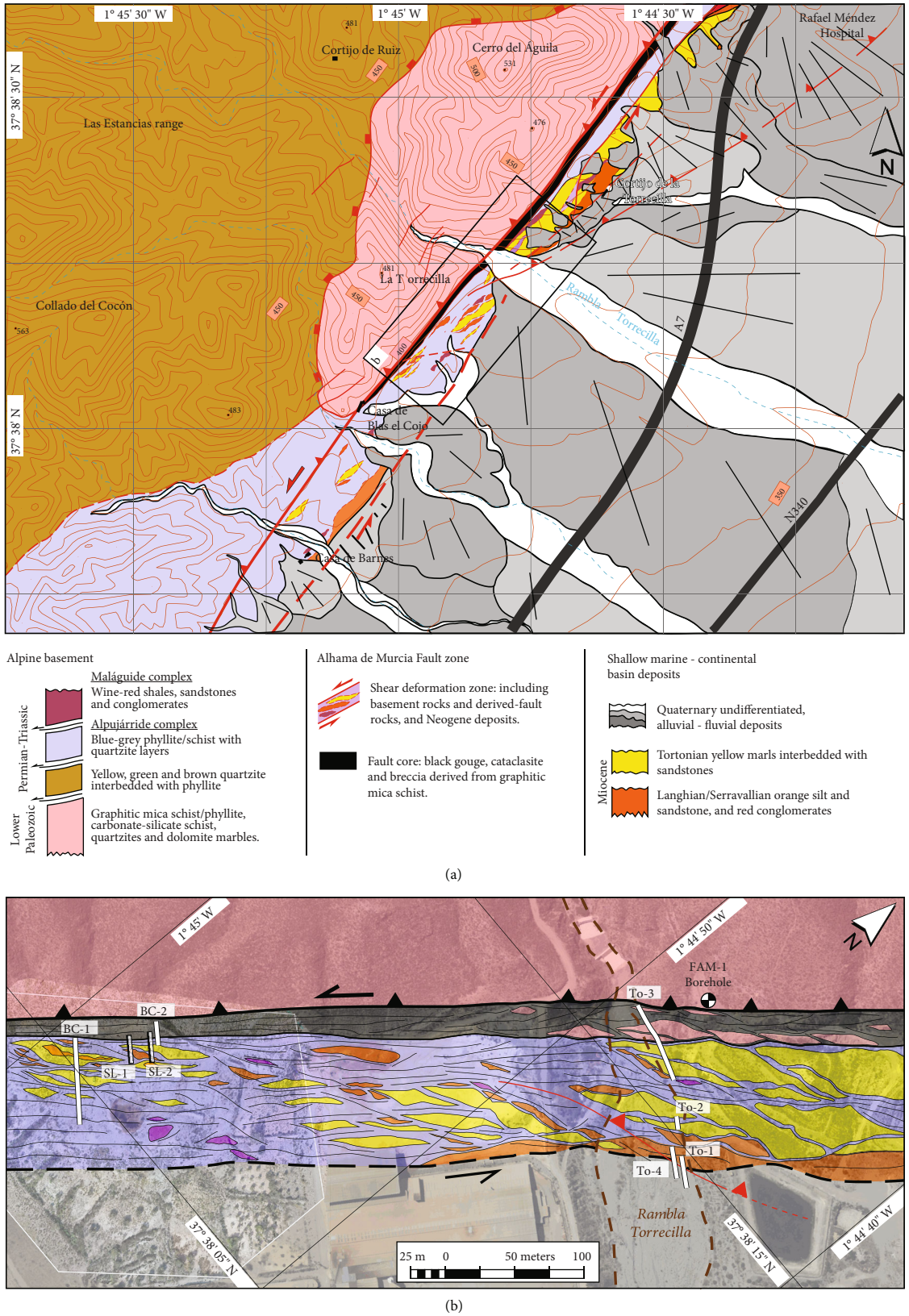

FIGURE 2: (a) Geological map of the study area at the northeast sector of the Goñar-Lorca segment of the Alhama de Murcia Fault (in red) and the 100 m wide shear zone. (b) Detailed map of the shear zone, dashed line is the lowest boundary of the shear zone; colors are protoliths involved. White lines with the labels To-1-4, BC-1-2, and SL-1-2 are the position of trenches and cleaned surfaces used in text. FAM-1 Borehole is the drilling location. Red fault trace is the surface rupture of 1674 catastrophic event mapping.

Units include locally Permo-Triassic Greywackes [57–59]. The sedimentary sequence in the study area is made of Neogene filling of the Lorca Basin: Lower-Middle Miocene (Langhian/Serravallian) Fluviodeltaic Conglomerates, Sandstones, and Limestones that locally overlie Foraminifera rich Marls [60, 61]; Upper Miocene transgressive sequence made of Conglomerates with clasts from Alpujarride Complex [62–64]; and Upper Miocene transgressive sequence is made of conglomerates with clasts from Alpujarride Complex [62–64]; Tortonian gray and yellow marls of Carivete Formation [60, 65] and an upper intercalation of several Messinian sedimentary environments recognizable of evaporitic gypsum and salts. Pliocene and Quaternary sediments are strictly related with the AMF activity: Pliocene Pleistocene Alluvial Fan related with mountain fronts and Quaternary alluvial deposits related with creeks [64, 66]. All these lithologies are involved in the shear zone, and their fabric is partially or totally overprinted by the Neotectonic fault activity (Figure 2).

3. Drilling, Trenching, and Sampling

This study is focused on La Torrecilla Site, where the AMF shows its clearest features and the fault rock is well restricted by previous studies [7, 20, 23–25, 43]. In 2015, a vertical borehole was drilled at this place (FAM-1 Borehole at Figure 2, [67]), and 174 m of drill core was sampled where almost a half was part of the fault rock. The high dip of the AMF (70°NW) made that the vertical borehole from the hanging wall crossed obliquely the fault zone and only sampled the upper domains of the fault rock (domain 1), but a continuous record of the transition between the hanging wall rocks and the fault core was obtained. In addition, in order to get a continuous record across the fault rock, six trenches were dug transversal to the fault zone structure, and two outcrop surfaces were cleaned. For an appropriate selection of trench sites, high-resolution aerial views from drone images were obtained, and field observation and detailed mapping of the shear zone were done previously to trench excavation (Figure 2(b)). Four of the trenches were made at "*La Torrecilla creek*" (To-1 to To-4), and two more trenches and two surface exposures were made 300 meters southwestward in an area named "*Blas el Cojo*" (trenches named BC-1 and BC-2, and surfaces SL-1 and SL-2). At *La Torrecilla* Site, Holocene sediments from La Torrecilla Creek cover most parts of the trenches, which was useful in order to assess the most recent increments of the deformation history of the shear zone. The trenches were cleaned and exhaustively measured and sampled; both oriented and nonoriented samples were taken. Trench photographs as logging are in the Supplementary Material; the summary of all the observations are in Figures 2 and 3; all the used outcrop scale pictures used in Figures 4–10 are sections of the trenches exposed in the Supplementary Material. Orientation data are also summarized in equal area lower hemisphere plots in Supplementary Material.

We have made 54 thin sections from the samples taken both in trenches and borehole, and some scanning electron microscope images were used focused on the fault core. The identification of deformation mechanisms and kinematic features and the fault rock classification were done using a polarized light optical microscope. The thin sections of unconsolidated samples were prepared by dry cutting after multicomponent resin primer. The studied sections of some samples were constricted by Toy et al. [9] method in order to constrain the Vorticity Normal Section [68]), but some of them are only vertical or horizontal sections of the fault rock. The used criteria to fault rock classification are the ones of Woodcock and Mort [69] that consider that matrix are all of those components smaller than 0.1 mm. The matrix/clasts proportion was obtained semiquantitatively using comparison charts for estimating percentage composition. The crystallographic preferred orientation (CPO) was qualitatively identified under cross polarized light and wave plate inserted. The shape preferred orientation (SPO) was measured in individual clasts or protoliths obtained from the division of major diameter by orthogonal minor diameter of a best fitting ellipse using Fiji software [70]. SEM observations were performed using a JSM 6335F SEMCamScan microscope operating at 10-20 kV and equipped with a Link System energy dispersive X-ray (EDAX) microanalyzer. One cm^3 irregularly fractured samples were dried using the successive procedure for unconsolidated sediments described by Tovey and Wong [71] and were prepared using epoxy resins and fresh surfaces coated with gold under vacuum.

4. Fault Rock Domains

We have distinguished five fault rock domains grouping lithologies or structural features across the shear zone. Here, we describe compositional and tectonite observations of each domain and the damage zone both at outcrop and microtectonic scale. All the descriptions are presented from the hanging wall to the footwall of the shear zone, being domain 1 the uppermost domain of the shear zone (closest to the hanging wall). The borehole FAM-1 is used mostly in the description of the shear zone boundary and domain 1; the rest of the classification is based on the trenches. All the observations are summarized in Table 1, their main microtectonic and outcrop features are presented in Figures 4–9, and their relative position is presented in Figure 3. The boundaries of the domains in some cases are sharp but some of them are gradual transitions of some properties of the fault rock (relative composition, matrix percentage, or deformation style) that are not a single plane; those boundaries should be taken as illustrative and variable along strike. This is the cases of domains 3, 4, and 5.

Several fault rock classifications are available based on relative amounts of matrix and clasts, the nature of matrix, grain growth, and cohesion among other criteria [72, 73]. Here, we used the nongenetic classification of Woodcock and Mort [69] for fault rock hand specimen that classifies the fault rocks according to three components: percentage of large clasts (>2 mm), small clasts (0.1 to 2 mm), and matrix or cement (<0.1 mm). The fault breccia are those fault rocks with more than 30% of large clasts, and three main subdivisions are distinguished: chaotic breccia (30-60% of large clasts), mosaic breccia (60 to 75% of large clasts), and crackle

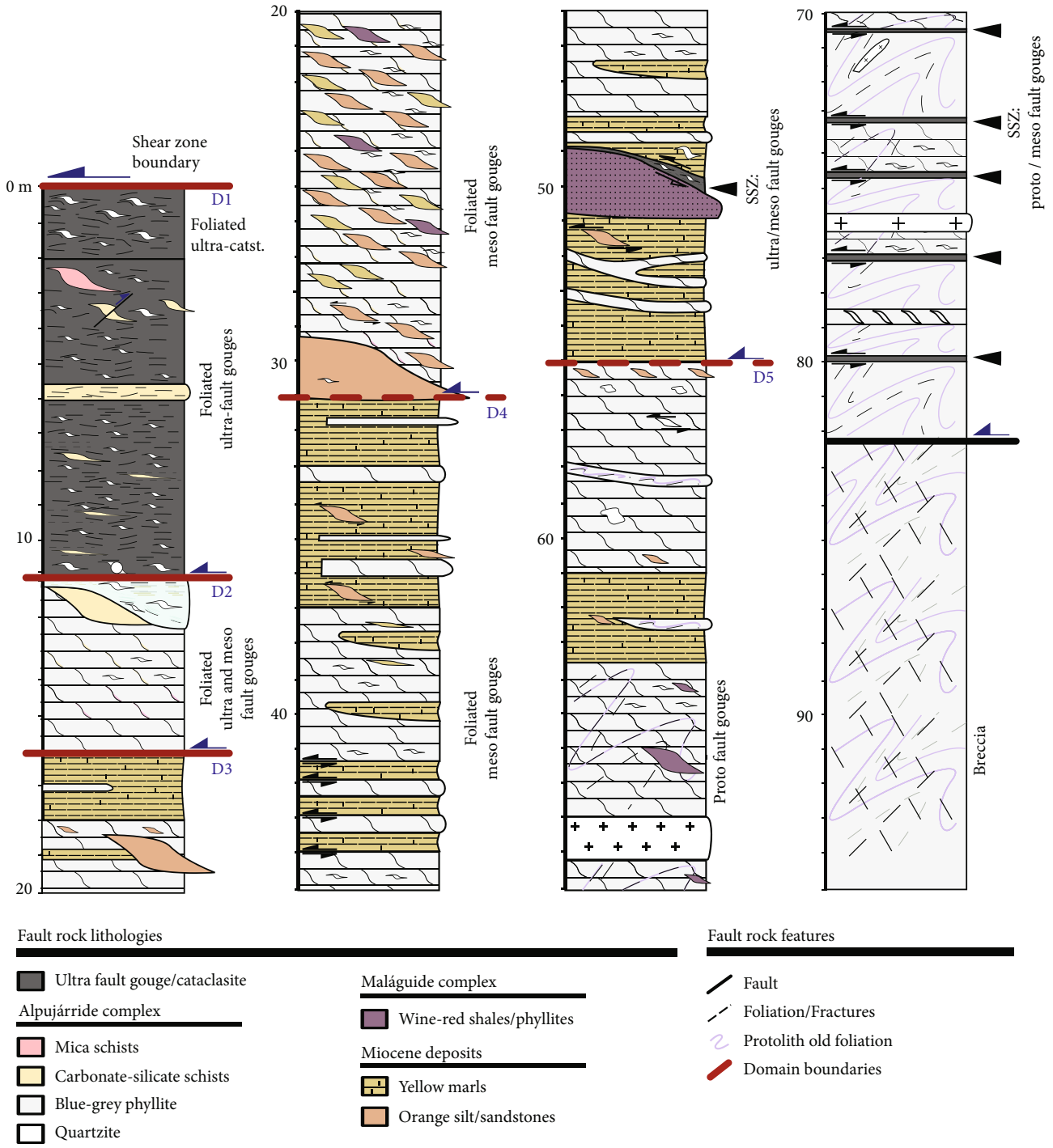

FIGURE 3: Synthesis column indicating domains relative positions, their thickness, protoliths, and shear indicators. D1 to D5 are the domains (separated by red lines). SSZ: Subsidiary Slip Zones.

breccia (large clasts >75%). When large clasts are less than 30%, we used the prefix proto-, meso-, or ultrafollowed by cataclasite or fault gouge in order to distinguish between fault rocks with a percentage of cement or matrix less than 50, between 50 and 90%, or greater than 90, respectively. If foliation is present, it is indicated in each case. If the fault rocks at present-day outcrop are cohesive, they are considered cataclasites, or fault gouges if incohesive. The protoliths involved in the fault rocks are also mentioned in each case.

4.1. Shear Zone Boundary. The shear zone boundary (SZB) at outcrop scale is sharp and discrete, and it is oriented 70/315. It puts the lower unit of the Alpujarride complex (Lower Paleozoic) in contact with the uppermost fault rock domain of the shear zone, which is a broadly studied black fault gouge here described as domain 1 (e.g., [20, 21, 23, 24]). At outcrop scale, the contact between both is solved in few centimeters and shows cleavage dip differences from 30° to 40°, but in some cases, we have identified thin fault gouges strands

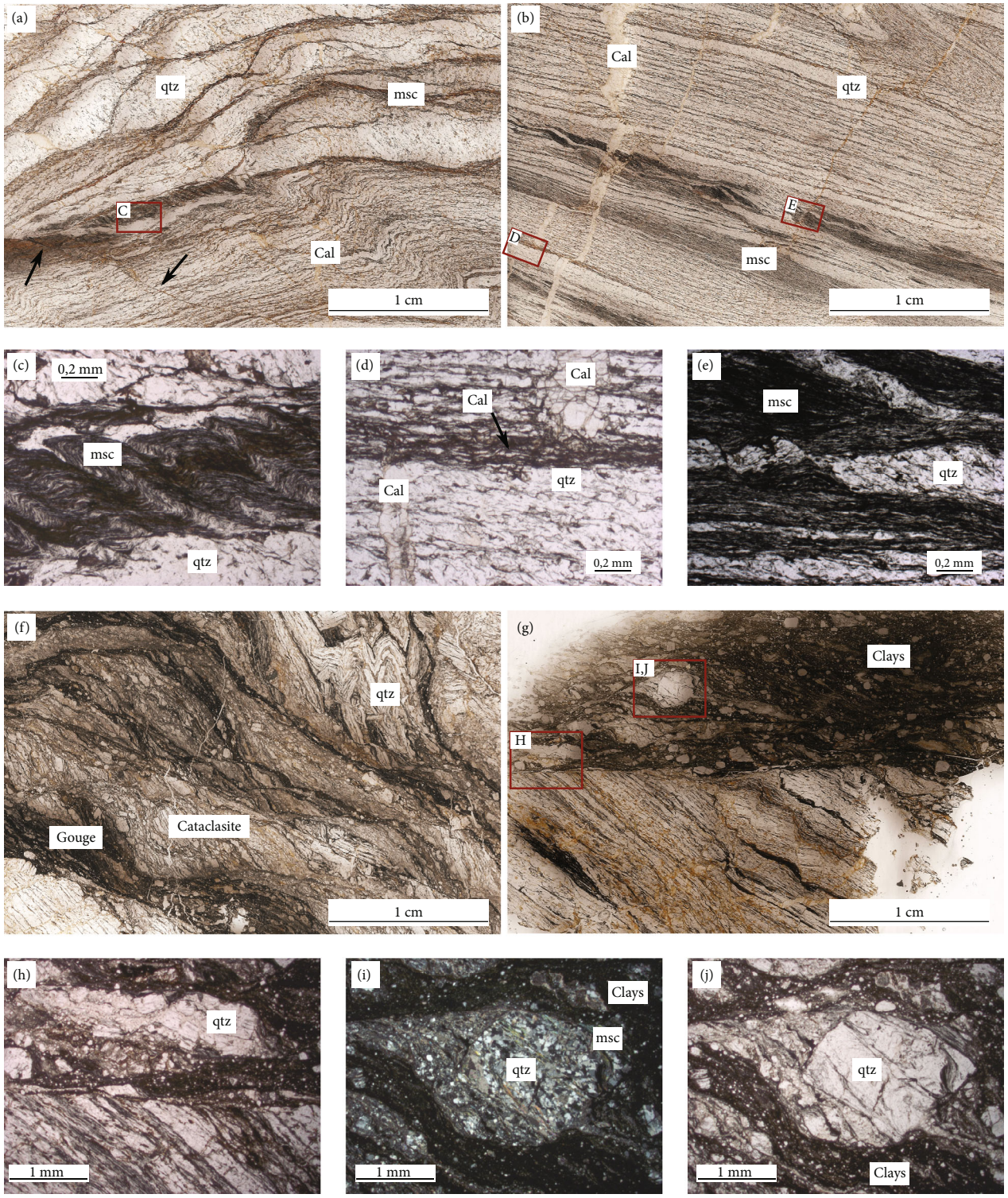

FIGURE 4: Microphotographs of the hanging wall damage zone and contact with shear zone. (a) Anastomosing cleavage and discrete transition to parallel cleavage in Lower Paleozoic Schists of the Alpujarride Complex at 1 m of the shear zone boundary. Arrows indicate brittle fractures parallel to axial plane foliation of the crenulation (detail in box C). (b) Lower Paleozoic Schists parallel cleavage and thin shear bands parallel to protolith cleavage; the darker aspect of the shear band is related with protolith comminution. (c) Crenulation with axial plane parallel to brittle fractures (inset in (a)). (d) Calcite vein offset and shear band involving some calcite clasts (inset in (b)). (e) Domino fractures in quartz rich microlithons (inset in (b)). (f) Gradational transition from schists to fault gouge. Anastomosed fault gouge bands and breccia overprinting Alpujarrde Schists. (g) Discrete contact of Lower Paleozoic Schists of the Alpujarride Complex and fault gouge (domain 1). (h–j) Details and kinematic indicators of the transition between protolith and fault rock (insets in (g)). Abbreviations used are qtz: quartz; msc; muscovite; cal: calcite; XPL crossed-polarized light.

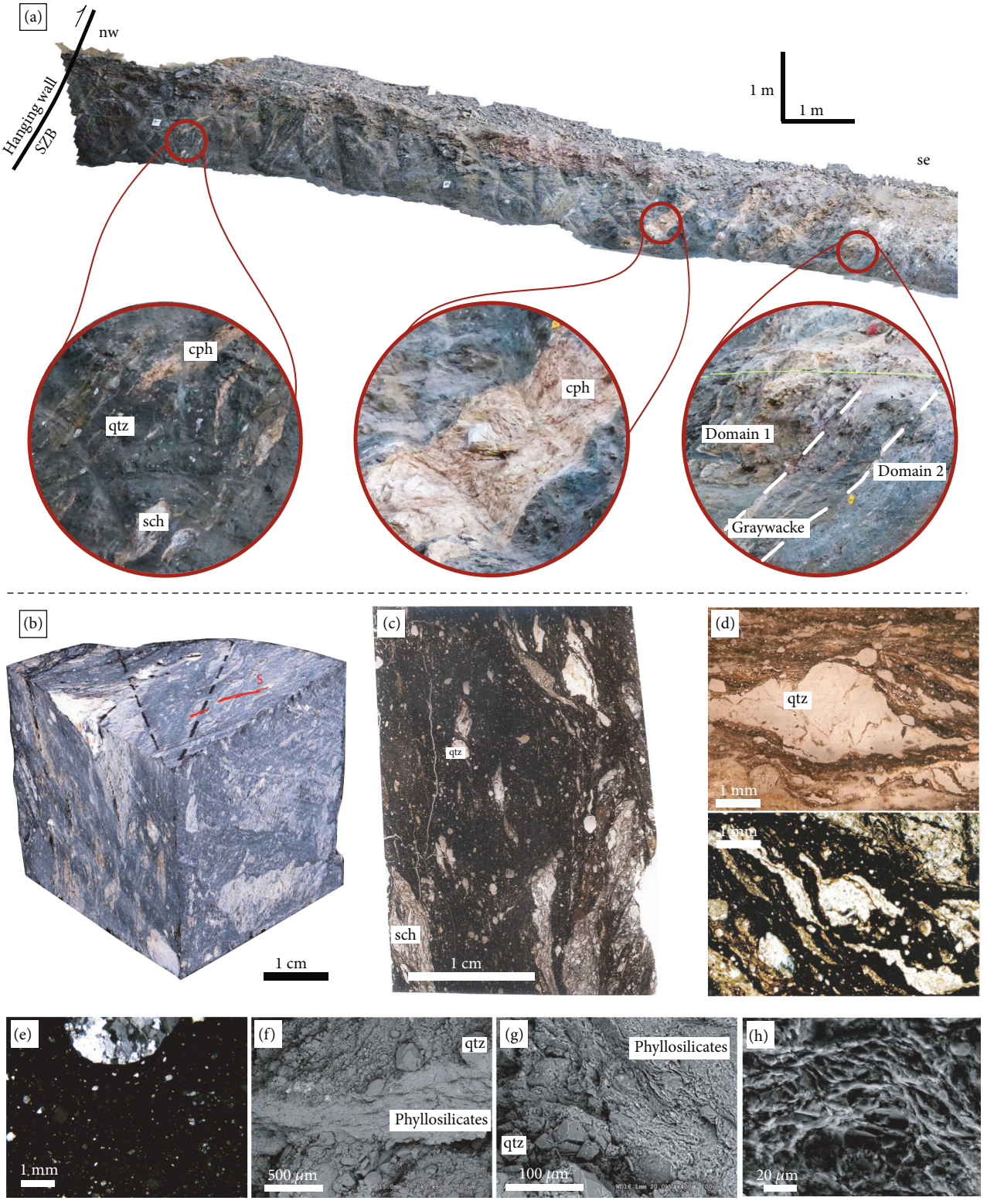

FIGURE 5: (a) Photo-log of the BC-2 trench showing the uppermost domain of the fault rock and its discrete contact with domain 2. SZB: Shear Zone Boundary. (b) Hand specimen from borehole; red line is cleavage. (c) Thin section of domain 1; the dark aspect of matrix is due to comminution and clay presence. (d) Details of the of the fault rock showing δ and σ objects. (e) Matrix detail with survivor submillimeter quartz clasts and clays. (f, g) Conchoidal fractures in microquartz and oriented phyllosilicates bounding quartz clasts. (h) S-C structures. Abbreviations are: sch: Schists; qtz: quartz: cph: calcite rich phyllites.

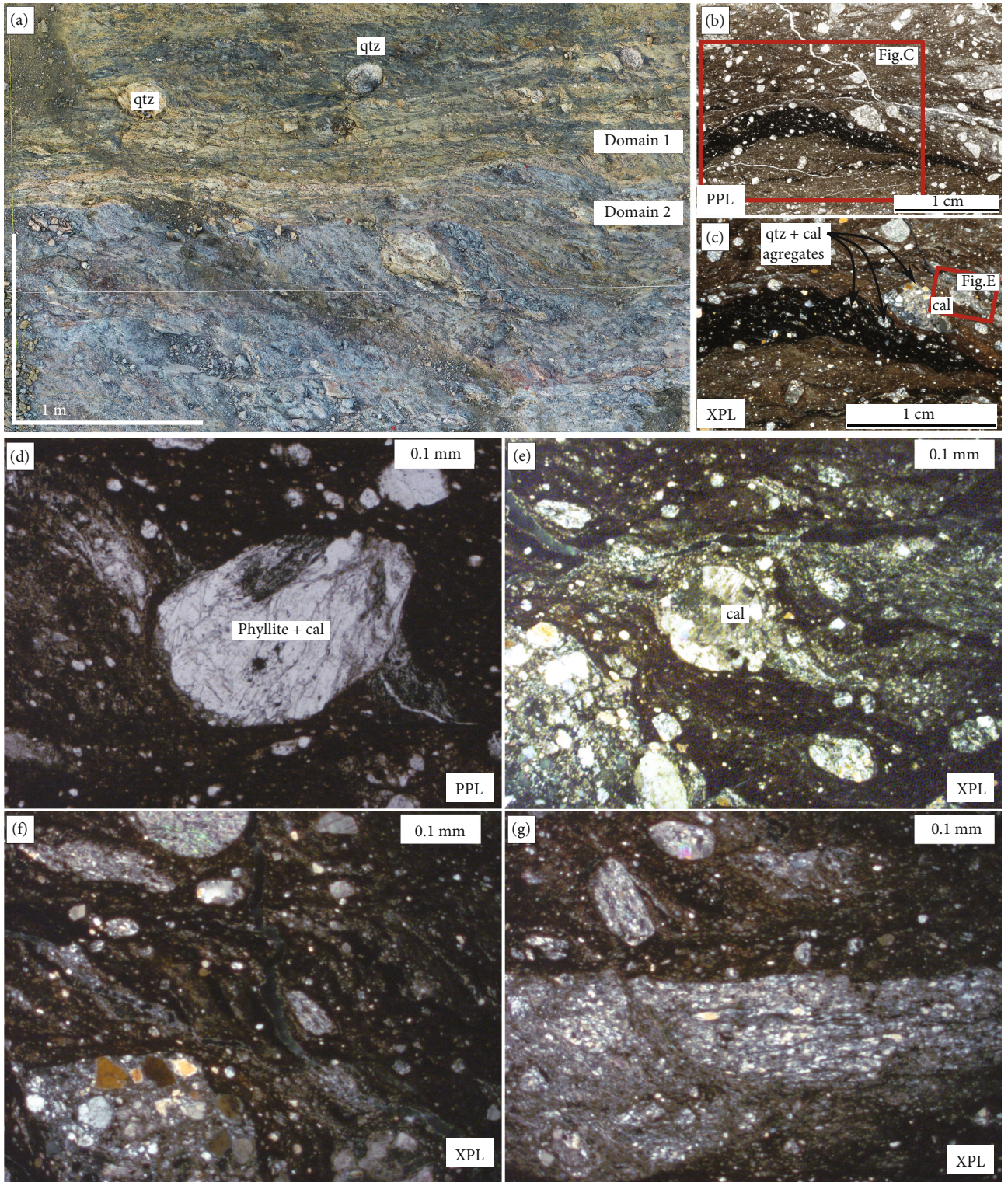

Figure 6: Main textural features of domain 2. (a) Photo-log of the surface SL-2 showing domains 1 and 2 discrete contact with two cleavage orientations. (b, c) Thin section of domain 2, fault gouge on gray phyllite, calcite, and quartz porphyroclasts in a clay enriched matrix. (d) δ object of a gray phyllite from upper Alpujarride Complex with calcite porphyroclasts. (e) σ object of calcite porphiroclast. (f) Quartz and calcite aggregate porphyroclasts and protolith profiroclasts showing SPO. (g) Comminution rounding a phyllite protolith. Abbreviations are PPL: parallel polarized light; XPL: cross polarized light; qtz: quartz; cal: calcite.

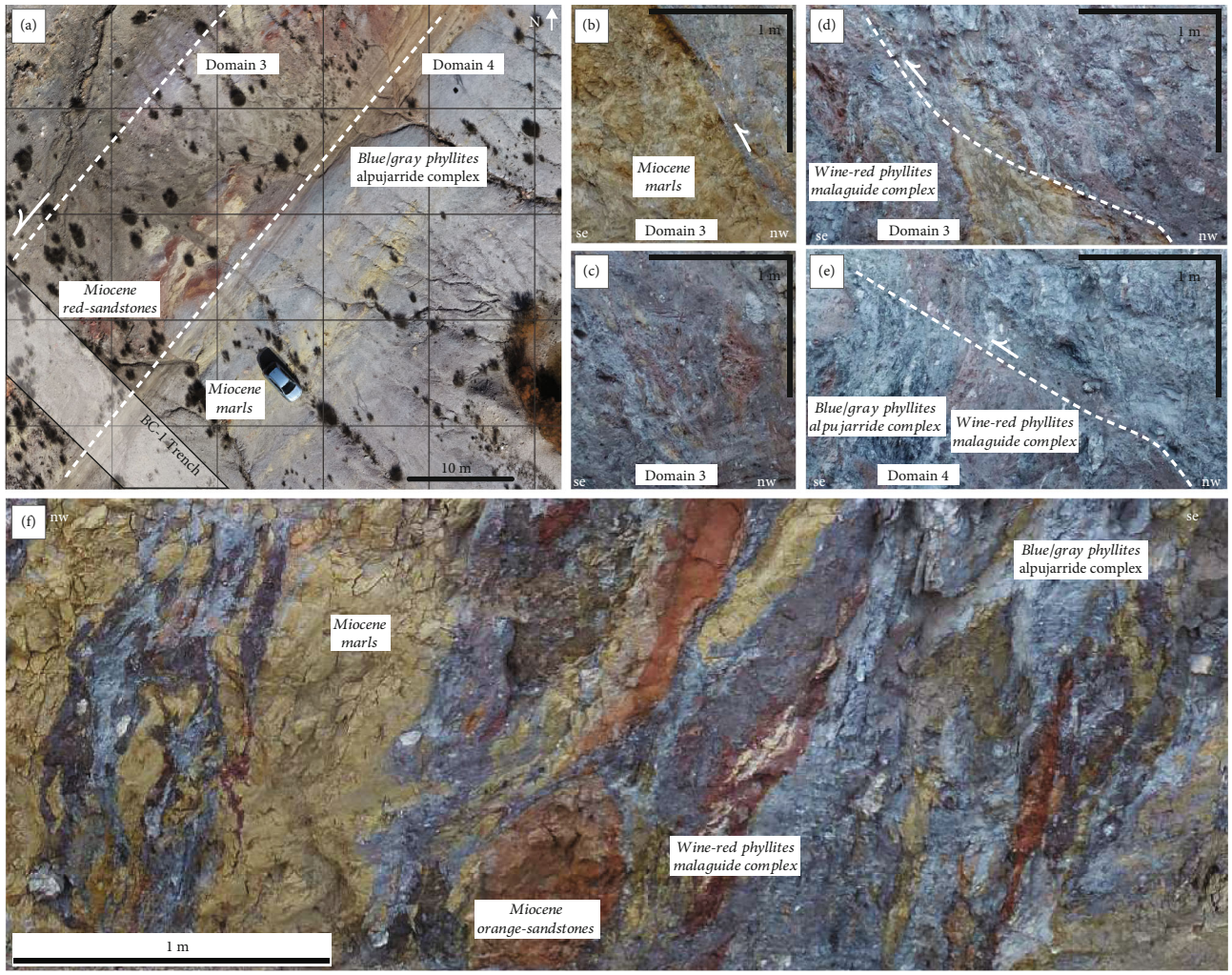

FIGURE 7: Domains 3 and 4 outcrop scale features. (a) Drone image of the surface previous to trench excavation showing gradational contact between domains 3 and 4. (b) Discrete contact between Marls and domain 2. (c) Alternation between Phyllites from Malaguide Complex, Phyllites from Alpujarride Complex and Marls. (d, e) Shears crosscutting the fault rocks. (f) Upper Alpujarride Phyllites, Malaguide Phyllites, Miocene Marls, and Sandstones involved in the shear zone.

(centimeter scale) of domain 1 parallel to the SZB few meters within the hanging wall that were used to define the hanging wall damage zone. At microscope scale, in the transition between the deformed and undeformed rock, we have identified evidence of reactivation of the schist fabric in at least 1 meter. In Figure 4(a), we show the original tectonic fabric of the Alpujarride Schist, with anastomosed cleavage that separates mica cleavage domains and quartz microlithons (at the upper part of microphotograph) and parallel zonal cleavage in the lower part with discrete boundary between them. We have identified thin shear bands parallel to the cleavage that offsets thin calcite veins (<0.01 mm wide) and some brittle fractures that offset cleavage domains (see Figure 4(b) and the detail in Figure 4(d)); in these offsets, some calcite porphyroclasts appear in the little shear zones that allow us to obviate refraction effects during vein injection. The crenulation cleavage is parallel to the SZB (detail in Figure 4(c)), and some quartz microlithons show domino fractures (Figure 4(e)). The dark aspect of some bands within the schist is interpreted as shear bands along the mica domains cleavage of the protolith, and their darkness is attributed to the presence of oxides and a drastic comminution of phyllisilicates during cataclasis processes that reactivated the original fabric. As the deformation increases, close to the SZB, protolith blocks are bounded by anastomosed gouge bands (Figure 4(f)) that in detail show sigma objects and S-C fabric (only visible at microscopic scale). Deformation also appears within the protolith blocks where we have identified shortening evidence reflected as chevron folds with thickened hinges and flexural slip in their limbs (upper-right corner of Figure 4(f)). In some cases, we have identified that the SZB is discrete as is shown in Figure 4(g), where we show a sharp contact between the hanging wall and the shear zone with intense deformation.

4.2. Domain 1: Homogeneous Foliated Ultrafault Gouges Overprinting Lower Paleozoic Schist. This domain is a black phyllosilicate/clay rich cataclastic matrix including lens-shaped fragments of schist/phyllite elongated parallel to the domain boundaries. Foliated ultrafault gouges are dominant,

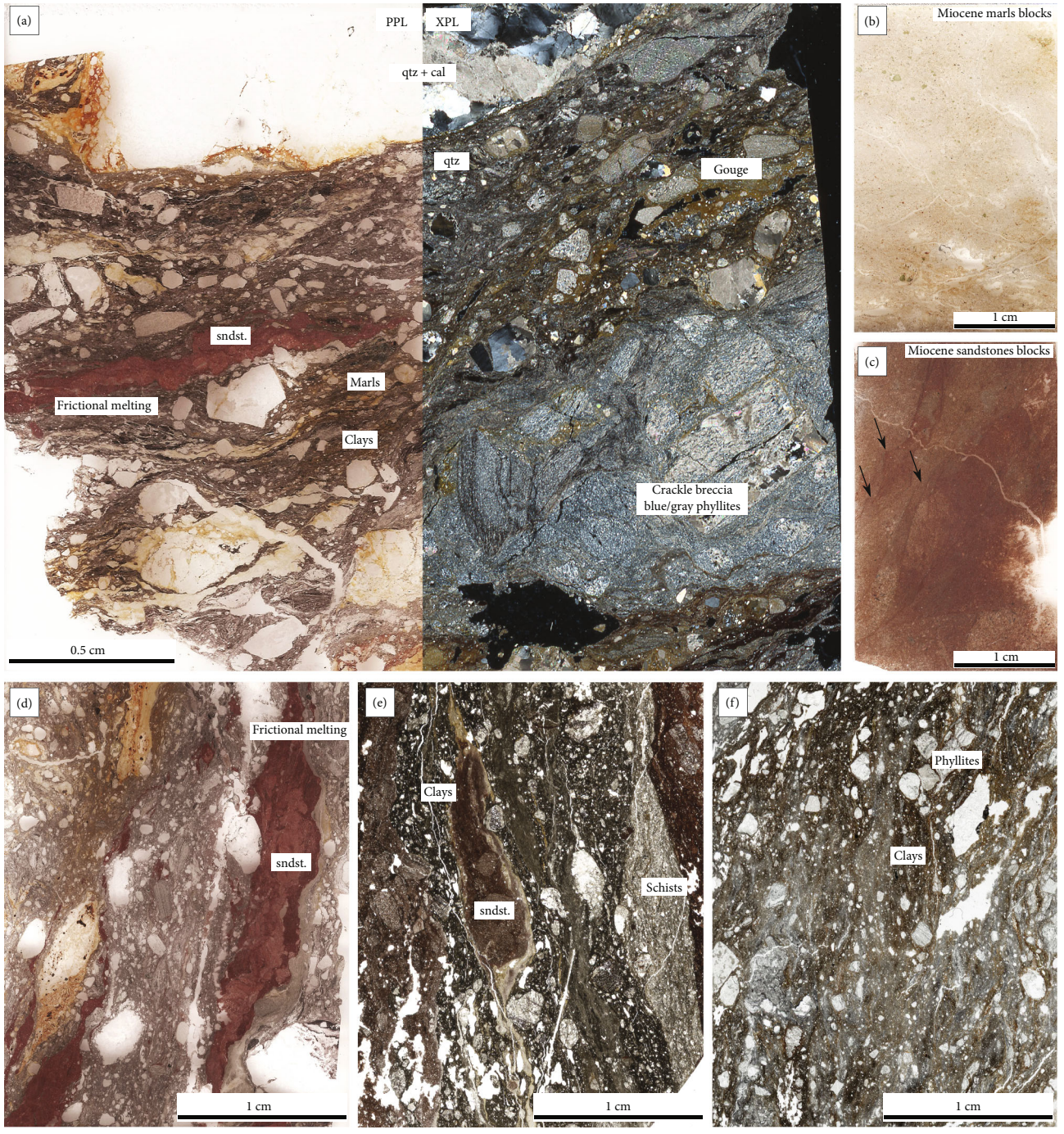

FIGURE 8: Domains 3 and 4 microtectonic features. (a) Thin section of cross polarized and parallel polarized light of domain 3 showing textural and compositional heterogeneities. (b, c) Thin sections of Sandstone and Miocene blocks in the shear zone showing some brittle fractures. (d) Cataclasites with frictional melting, related with Miocene sandstone protolith. (e) Subsidiary Slip Zone in domain 4. (f) Domain 4 foliated mesocataclasite. Abbreviations are PPL: parallel polarized light; XPL: cross polarized light; qtz: quartz; cal: calcite; sndst: sandstone.

but other rock units as breccias and distorted schists/phyllites are found close to the embedded protolith blocks representing different stages of deformation. This domain has been studied by several authors (p.e. [20, 23–25]). At outcrop scale, this domain is a 10 to 30 meters wide gouges with S-C and S-C' structures including quartz and schists lenses (Figures 3 and 5). In the first two meters, in the area closer to the SZB, foliated and cemented ultracataclasites appear (less than 30% of clasts higher than 2 mm and more than 90% of fine grained (clay) matrix); within this first 2 meters, the only protolith is the Alpujarride Graphitic mica schist. From meter 2, towards the footwall, some calcite rich phyllites appear (from the lower unit of the Alpujarride Complex) forming lenses within the fault rock that in some cases show

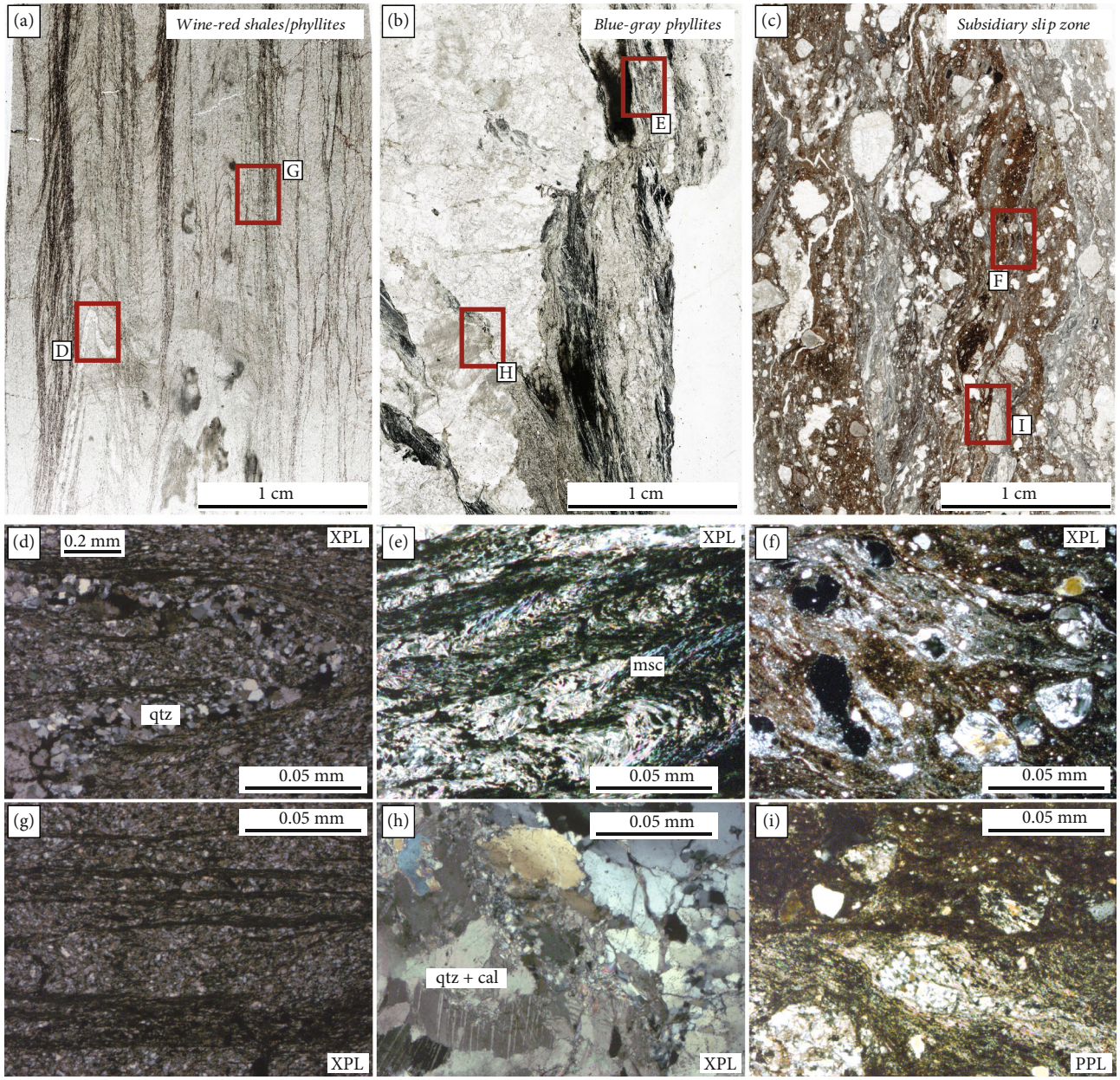

Figure 9: Domain 5 microtectonic features. (a, d, and g) Thin section of wine-red Malaguide Complex phyllites with slight features of neotectonic overprinting fabric. (b, e, and h) Thin section of Blue/Gray Alpujarride Phyllites with some features of the overprinting neotectonic tectonite fabric. (c, f, and i) Subsidiary Slip Zone, meso-cataclasites within domain 5; here, the only protolith found are the Blue-Gray Phyllites. Abbreviatios are PPL: parallel polarized light; XPL: cross polarized light; qtz: quartz; cal: calcite; msc: muscovite.

their original cleavage but it is mostly overprinted by foliated ultrafault gouges. From meter 7, the black fault gouge is dominant again, and some evidence of discrete fault planes starts to appear. Close to the boundary with domain 2, some 10 to 20 centimeters diameter quartz delta and sigma porphyroclasts appear all parallel to the SZB indicating simple shear sense. The boundary with the next domain is sharp and parallel to the shear zone boundary, with rotated foliation that is also parallel to the SZB which is indicative of intense deformation (Figure 5(a)).

At optical microscopic scale petrographic analysis of samples from domain 1 together with XRD and SEM analysis performed by Rutter et al. [20] and Rodriguez-Escudero [43], they confirm that all rock units derived mainly from mechanical fragmentation of schists from the lower unit of the Alpujárride Complex. Mineralogy of wall rocks and derived fault rocks is predominantly composed of quartz and white mica (muscovite, illite, and paragonite), with the gouges/cataclasites being enriched in clay fraction compared to the protolith (Figures 5(c) and 5(d)). Geometric structure of the rock unit is systematic over the range of studied scales, from outcrop to SEM. Gouges/cataclasites occur in a network of C and C' shear bands enclosing lens-shaped fragments of protolith and quartz (Figures 5(c) and 5(h)). Arrays of distorted schists

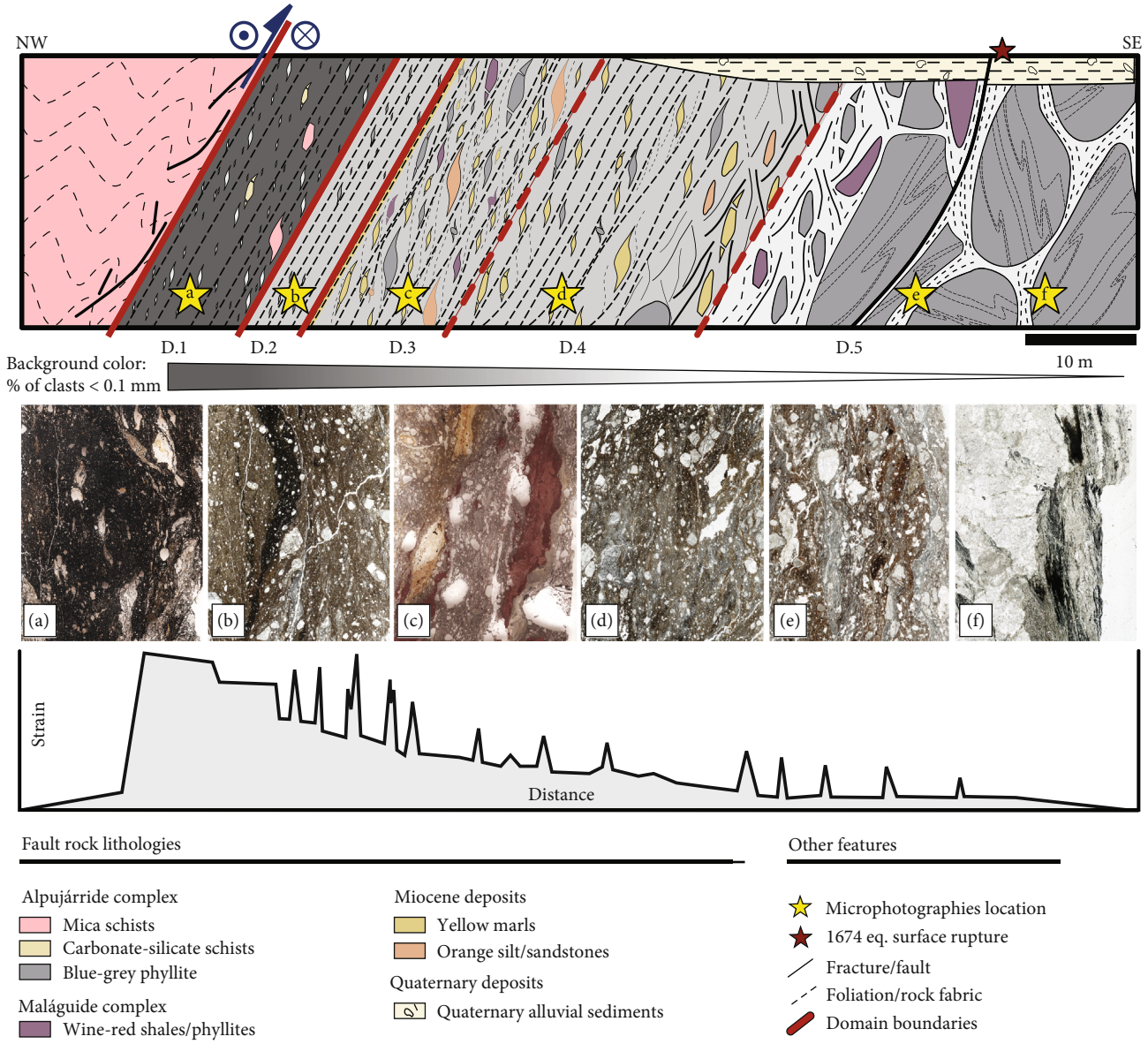

FIGURE 10: Synoptic sketch of the fault zone architecture and strain distribution. D.1 to D.5 are the domains. Yellow stars show the position of the thin section in lower part. Thick black lines within the hosting rock represent hanging wall damage zone; thin lines represent host rock original fabric. Note that faulting offsets Quaternary sediments over domain 5. Curve shows strain vs. distance across the shear zone qualitative distribution.

and breccia are typically located in pressure shadows of the wall rock fragments. Breccia are composed of angular to subangular clasts of schists in a finer-grained matrix which is often cemented. Distorted schists correspond to protolith fragments affected by a dense network of oriented fractures leading to a prominent loss of cohesion, but original structures are clearly recognizable. Precipitation of carbonates and iron oxides is common along fractures in protolith fragments and coarse-grained rock units, leading to reddish to brown discolouring (Figures 5(b) and 5(d)).

The very fine-grained nature of the gouge matrix means that it appears black when viewed under an optical microscope in crossed-polarized light (Figure 5(e)). Gouge/cataclasite shows grains down to about 200 μm. However, these grains are clasts belonging to a matrix-based fabric of even smaller particles (<50 μm) mainly composed of preferentially oriented phyllosilicates/clays and isolated subangular to subrounded quartz grains (or survivor grains, Figures 5(f) and 5(g)). Gouge frequently incorporates asymmetric schist clasts and pulverized quartz clasts (>>2 mm), which are oriented parallel to the foliation. While schist clasts are regularly sheared along gouge-internal shears, there is no obvious preferred orientation of the fractures in the quartz clasts, suggesting that they may result from coseismic pulverization as stated in [24]. On the other hand, in the arrays of distorted schists and breccias located in pressure shadows of sigmoid, there is slightly Crystal Preferred Orientation (CPO), which is not evident in protoliths.

Table 1: Summary of the deformation domains of the Alhama de Murcia Fault Rock.

Domain	Classification	Protolith (s)	Brief description	Mineralogy	Def. mechanisms	Notes	Figure
1	Foliated ultrafault gouges and ultracataclasites.	↑ ↑ Lower Paleozoic Alpujarride Complex Graphite rich Schists Calcite rich phyllites	Black phyllosilicate/clay rich cataclastic matrix including lens-shaped fragments of schists elongated parallel to the domain boundaries. S-C S-C' fabric. First two-meter cohesive rocks. Remaining incohesive. Disperse schists forming horses. Strong lateral continuity.	Quartz, muscovite, illite, paragonite, graphite, kaolinite, ↓↓calcite	Mechanical fragmentation Cataclastic flow Frictional sliding Quartz powdering	Sharp boundaries, slight crystal preferred orientation in quartz tails.	Figures 4 and 5
2	Foliated ultra- and mesofault gouges	↑Permo-Triasic Fine Grained Blue /Gray Phyllites. ↓Calcite rich Phyllites. ↓↓↓Disperse fragments of Langhian/Serravallian reddish/ orange silts and sandstones	Incohesive pyllosilicate/clay rich cataclastic matrix with centimeter scale quartz, phyllite and calcite porphyroclasts forming S-C S-C' tectonite. Strong lateral continuity.	Quartz, calcite, illite. Some alteration minerals appears (possibly Fe and Ti oxides)	Cataclastic flow Frictional sliding	Clear CPO in calcite sigmoid tails. SPO of phyllite subhedral porphyroclasts.	Figure 6
3	Foliated meso- and protofault gouges. Marls and sandstones breccia horses	↑↑Tortonian yellow marls ↑↑Permo-Triasic Fine Grained Blue /Gray Phyllites. ↑Langhian/Serravallian silts and orange sandstones ↑Wine-red shales and sandstones from Triassic Malaguide Complex	Anastomosed shears of meso/protofault gouges clay enriched matrix with heterogeneous protolith lenses forming S-C structures. Higher comminution located in anastomosed shears bounding protoliths blocks. Heterogeneous alternate of anastomosed gouges overprinting blue/gray phyllites, marls and sandstones.	Quartz, illite, paragonite, calcite, chlorite, smectite. Some opaques (possibly Ti and Fe oxides)	Cataclastic flow Frictional sliding ↓ ? Frictional melting	Corroded boundaries of some injection like structures point to frictional melting, only visible at microscope scale- mostly related with snadstones.	Figures 7 and 8
4	Foliated meso- and protofault gouges.	↑↑Tortonian yellow marls ↑↑Permo-Triasic Fine Grained Blue-Gray Phyllites. ↓Langhian/Serravallian silts and orange sandstones ↓Wine-red shales and sandstones from Triassic Malaguide Complex	Meso/protofault gouges clay enriched matrix with herterogeneus protolith lenses forming S-C structures. Homogeneous alternate of anastomosed gouges overprinting blue-gray phyllites and marls	Quartz, muscovite, illite, smectite, calcite. Some opaques (possibly Ti and Fe oxides)	Cataclastic flow Frictional sliding ↓ ? Frictional melting	Gradual upper and lower limits	Figures 7 and 8

Table 1: Continued.

Domain	Classification	Protolith (s)	Brief description	Mineralogy	Def. mechanisms	Notes	Figure
5	Foliated protofault gouges and breccia	↑↑Permo-Triasic Fine Grained Blue-Gray Phyllites. ↓Wine-red shales and sandstones from Triassic Malaguide Complex	Derived fault rocks show less or circa 50% of matrix and are mostly composed by mica and comminuted clasts from Upper Alpujarride Blue/Gray Phyllites	Quartz, calcite, illite. Some alteration minerals appears (possibly Fe and Ti oxides)	Cataclastic flow Frictional sliding	Old tectonite fabric is evident. There are a lot of intact blocks of Alpujarride Phyllites with anastomosed thin shear zones enclosing them.	Figure 9

4.3. Domain 2: Homogeneous Foliated Ultra- and Mesofault Gouges Overprinting Blue/Gray Phyllites. Four meters wide domain of ultra/mesofoliated fault gouges overprinting Blue/Gray Phyllites with quartzite layers from upper units of the Alpujarride Complex (Figure 3). Incohesive fault rock with approximately 30% of clasts higher than 2 mm and more than 50% of clay rich matrix form S-C/S-C' structures with centimeter scale quartz and phyllite porphyroclasts. In the upper part of domain 2, we still observe some porphyroclasts of calcophyllites that disappear downward. Some disperse fragments of reddish/orange silts and sandstones from Langhian/Serravallian Miocene Units appear. In the most northeastern part of our excavations, an exotic thin level of fault rocks appear overprinting Devonic-Carboniferous greywackes (trench 2 and surface 2, Supplementary material and Figure 5). At outcrop scale, it is possible to identify the original Blue/Gray Phyllites tectonic fabric with the overprinting neotectonic S-C and S-C' fabric.

At microscopic scale, we have identified mineralogy coming from Alpujarride phyllites, white mica, and quartz in the gouge enriched of clay. Calcite is abundant at this point and some opaque mineral appears (possibly Fe and Ti Oxides). Matrix is composed of survivor quartz clasts and clay minerals (illite) from protolith comminution. Calcite is present both in veins with tabular thick twins and as sigmoids clasts with strong CPO in their tails. Quartz is also abundant forming porphyroclasts and/or crystal aggregates. The quartz porphyroclasts show undulose extinction surely inherited from original tectonite. The fine grain matrix is composed of clay minerals but also of tiny quartz and calcite clasts with slightly CPO. The comminution at this point is lower than in domain 1 but still effective with more than 70% of clasts lower than 0.1 mm and in some areas even more. The porphyroclasts have aspect ratio ranging from 2 to 2.5 and showing shape preferred orientation with long axes mainly oriented parallel to foliation (Figure 6(f)) or C shears (Figure 6(g)). Chaotic microfractures are predominantly within protolith lenses being part of cataclasis or comminution during shearing.

4.4. Domains 3 and 4: Heterogeneous Mixture of Paleozoic, Permian-Triassic, and Miocene Protoliths. From this point, the deformation became more spatially heterogeneous, and the domain classification is based on gradual changes in relative compositions of protoliths (boundary between domains 3 and 4) or the deformation intensity (boundary between domains 4 and 5). We have unified the description of domains 3 and 4 in the same section because their only difference is the relative amount of the protoliths, specifically the Blue/Gray Phyllites that became dominant within domain 4. The boundary is gradual, and it could be located in a broad band (few meters wide) across the strike of the shear zone. Even more, these units, together with domain 5, change their width along strike.

Domains 3 and 4 are heterogeneous domains of fault gouges mixing and overprinting yellow marls, silts, and sandstones from Miocene, wine-red shales, and sandstones from Triassic Malaguide Complex and Blue/Gray Phyllites from Permian-Triassic Alpujárride Complex (Figure 3). The upper boundary of domain 3 is a sharp contact between domain 2 and Miocene Marls lenses with low quantity of internal kinematic markers (Figures 7(a), 7(b), and 8(b)). The orientation of the marls lenses has been identified in their boundaries, where phyllites appear (oriented almost parallel to the SZB 60/310). Some lineations are preserved in this unit with chaotic plunges pointing to complexities in deformation style (orientation data are available in Supplementary Material (available here)). At this point (at outcrop scale), the comminution of Blue/Gray Phyllites is still effective developing a cataclastic matrix of more than 50% of the fault gouges. From meter 18, some Triassic sandstone and silt blocks start to appear (meter scale at the top to centimeter scale to the bottom, Figure 3) with sigma and delta shapes indicating simple shear sense (Figure 7(f)). This alternation is constant from meter apx. 18 to meter apx. 31 where Malaguide Sandstone Blocks appear. In the boundaries of the blocks, slip is concentrated, and comminution processes had been more intense forming gouges (Figure 8(e)). The boundary between domains 3 and 4 has been established close to meter 30 from the hanging wall in a Malaguide Complex Block bounded by well-developed gouges that we have defined as Subsidiary Slip Zone (SSZ). From this point, the deformation is characterized by an anastomosed alternation between gouges overprinting centimeter to decimeter scale Blue/Gray Phyllites and marls bands. The sandstone blocks are less abundant, but when appear, they are bounded by penetrative tectonic fabric developing foliated mesofault gouges overprinting the Blue-Gray Phyllites.

At optical microscope scale, the observations in these domains are redundant with the features identified at outcrop scale. Thin sections of lenses or blocks from Miocene deposits (Tortonian yellow marls or Langhian/Serravallian orange silts) show unaltered mineralogy, calcite marls, and foraminifera or quartz-rich fine-grained silt. The studied thin sections of the marls domains do not show clear evidence of internal deformation apart from some isotropic fractures. Some fossil appear (foraminifera) within Marls units, and microfractures are present in both with no remarkable features (Figures 8(b) and 8(c)). Thin sections of the most heterogeneous area (located in the area of Figure 7(f) at around meters 20–30 from the hanging wall) show gouge bands with centimeter to millimeter quartz/phyllites or sandstone lenses porphyroclasts. The clay-rich matrix is mainly composed of white mica and illite with some quartz fragments coming mostly from mechanical comminution of phyllites. Calcite is also abundant as porphyroclasts or vein injection. Some opaque mineral appears overlapping all the deformation (surely alteration minerals). Corroded boundaries and vein injections of apparently devitrified material bounding some sandstone clasts are interpreted as evidence of frictional melting (Figures 8(a) and 8(d)). Shape preferred orientation of clasts and S-C and S-C' structures are common in the gouge bands. Compared with the other domains, here, the fault rocks show a relative increase in C' shears. Quartz porphyroclasts have rounded boundaries that indicate mechanic fragmentation, with an aspect ratio around 2 with long axes mostly oriented parallel to C' shears; the phyllite porphyroclasts have a higher aspect ratio (>2.5) and higher angularity with long axis orientation consistent with the

quartz porphyroclasts. Same feature has been identified at the boundaries of blocks where slip is concentrated along gouge bands forming SSZ, where the deformation is more intense than the bounding planes (Figure 8(e)).

4.5. Domain 5: Fault Gouges Bounding Lenses of Variably Deformed Protoliths. Foliated protofault gouges and crackle breccia overprint Blue/Gray Alpujarride phyllites and red-wine Malaguide shales/phyllites. At this point, the old tectonite fabric is evident, and the overprinting neotectonic fabric and comminution has not been efficient yet (Figures 9(a) and 9(b)). Derived fault rocks show less or circa 50% of matrix and are mostly composed by mica and comminuted clasts from Upper Alpujarride Blue/Gray Phyllites. There are many intact blocks of Alpujarride Phyllites with some alterations and faults and fractures crossing them. Until meter 65 to the hanging wall, there is still some alternation with Miocene Marls lenses. From meter 70, almost all the deformation is located in discrete bands bounding intact blocks, with S1 oriented 70/025; 70/010 (Figures 3 and 9(c), and Supplementary Material for stereoplots showing orientation data). In the discrete shear zones, protofault gouges are developed, with powdered quartz clasts and S-C fabric (Figures 9(f) and 9(i)); towards the footwall of the shear zone, the crackle breccia is more common (mostly overprinting veins), and mosaic breccia overprinting phyllites appears in the protolith blocks (Figures 9(b) and 9(h)), and the gouge strands are less abundant. We found displacement evidence in single and narrow shear bands of fault gouges oriented parallel to axial plane crenullation foliation overprinting the Blue/Gray Phyllites where the original tectonite has not been completely overprinted. In some bands (apx. 1 to 10 cm wide) within domain 5 comminution has been effective enough and almost completely overprinted old fabric. These shear bands are classified as SSZ that seem to reflect the last increment of deformation of the historical record as we discuss below.

At microscale, the identified mineralogy is the same of the protoliths; there is a clay enrichment only in SSZs. The blocks of Red-Wine Phyllites from Malaguide Complex show spaced parallel cleavage, with cleavage domains of white mica and microlithons mostly composed by quartz. At the microlithons, there are some folds with axial plane parallel to cleavage (Figures 9(a), 9(d), and 9(g)). Within the Blue-Gray Phyllites blocks, some brittle fractures are identified, and crackle breccias are overprinting mostly quartz and calcite aggregates. At the boundaries of the quartz veins, there is more intense cleavage (cleavage percentage domains increase, Figures 9(e) and 9(h)). The identified SSZ gouges have same mineralogy as their protoliths, clay enriched matrix with quartz and phyllite porphyroclasts. They show S-C S-C' structures with sigma and delta porphyroclasts with aspect ratio around 1.5–2 and angular boundaries. Shape preferred orientation is present with the long axes oriented parallel to the boundaries of the SSZ (Figure 9(c), 9(f), and 9(i)).

5. Discussion

5.1. On Textures and Slip Distribution (from Core to Surface Rupture of Historical Events). The textural and petrographic analyses of fault rocks across the AMF fault zone, including FAM-1 borehole data, six trenches excavation, and two cleaned surfaces, reveal a strongly heterogeneous shear zone regarding to its compositional and structural features. It ranges from the fault core rocks in domain 1 (derived from Paleozoic schist), where strain is distributed within several meters wide of foliated ultrafault gouges and ultracataclasites, to domain 5, where strain is concentrated along discrete fault planes (or shear bands) involving Permian-Triassic to Holocene rocks. Even we have identified corroded borders (pointing to frictional melting) and slightly crystal preferred orientation in some units (maybe pointing to intracristaline dislocations), cataclasis, cataclastic flow, and frictional sliding are the dominant deformation mechanisms during shearing. Blenkinsop [74] showed that the fractal dimension of the Particle Size Distribution depends on several features such as fragmentation process, initial size distribution, number of fracture events, energy input, strain, and confining pressure, and it is increased by last four. Thereby, considering matrix the proportion of clasts lower than 0.1 mm, the percentage of matrix can be used as a qualitative *proxy* to identify the relative degree of incremental deformation that each domain had accommodated, even more when they have the same protolith, which is the case of the Blue/Gray Phyllites that appears across almost the whole shear zone. Within each domain, it is possible to find more than one kind of fault rock (i.e., within domain 1, we found foliated ultracataclasites and gouges but eventually some fault breccia appears; or in domains 3, 4, and 5 where protofault gouges and breccia are dominant but some shear planes show an increase in their matrix percentage compared with the surrounding rocks). However, the fault rock classification of major features of each domain shows that there is a decreasing trend in the percentage of matrix (clasts lower than 0.1 mm) from the hanging wall to the footwall of the shear zone. This could be pointing to a decrease in the accommodated strain from the upper parts of the shear zone (domains closer to the hanging wall, where foliated ultrafault gouges are dominant) towards the footwall (where protofault gouges and breccia are dominant) (Figure 10).

The uppermost unit (domain 1) is composed mostly of the lower tectono-stratigraphic unit, the Paleozoic Alpujarride Schists, which is considered to have more accommodated strain and here classified as the fault core. This is consistent with its textural features here classified as foliated ultrafault gouges, where the original (old) tectonic fabric of the protolith had been almost completely overprinted. Domain 2, which is composed of upper units of the Alpujarride Complex, is texturally homogeneous, and its structural style has features close to the identified in domain 1 but with a relative decrease in the matrix percentage (here lower but close to 90%) and thereby classified as a foliated (meso) fault gouge. We propose that the textural differences between domains 1 and 2 are due to different stages of the comminution processes, that are in an earlier stage in domain 2 than in domain 1, which is maybe in a steady stage (which is also consistent with the kinematic analyses done in domain 1 in [25]). The intensity of the deformation in domain 2, its lateral continuity, and homogeneity make us to include it in the fault core.

From domain 3, there is a heterogeneity increase in both textural and petrographic features but a decrease in the accommodated slip. From domain 3 to domain 5, the slip (strain) is mostly accommodated in areas where there is a constant intercalation between protoliths (microphotograph (c) in Figure 10), but with a relative increase in some slip zones bounding bigger blocks. When the size of the different protolith blocks is constant the slip is distributed in wider areas, but when bigger blocks appear (decametric scale), the slip is more concentrated in anastomossed shear zones of meso- and protofault gouges bounding the blocks. Some of the studied blocks show only some microfractures, while in their boundaries, we have identified foliated fault gouges. Domain 4 is in gradual contact with both domains 3 and 5 and is composed of mostly an alternate of Miocene Marls and Upper Paleozoic Blue/Gray Phyllites. Here, the matrix percentage is around a 60% (mesofault gouges), decreasing towards the footwall of the shear zone, until the protolith tectonic fabric is evident, criteria followed to distinguish between domains 4 and 5. Within domain 5, the slip (strain) is preferentially (but not only) accommodated in some anastomosed slip zones (SSZ, classified as meso-fault gouges), bounding Alpujarride and Malaguide Complexes protolith blocks with their original fabric not overprinted yet (Figure 10).

We propose that, from domain 3, the mechanical heterogeneities of the different protoliths may had conditioned the heterogeneity in the slip distribution and the competency contrast favors slip in the block boundaries [75]. This fact is visible both at outcrop scale and microscope scale, where we found that within the protolith blocks, there is almost no cataclasis (apart from some microfractures) while out we find gouges (see Figure 8(a)). The low-lateral continuity of these domains and their internal heterogeneities in both deformation intensity and lithology make us to classify them as a highly intense deformed damage zone. A similar process was describe by Fagereng and Sibson (2010) for shear displacements in subduction channel where the deformation within a melange is concentrated in the contact between incompetent and competent materials, with shear bands localized along lithological contacts or within competent materials while the matrix flow accommodate strain as distributed deformation.

The SSZs within domain 5 or domains laterally equivalent (possibly lateral continuation of domains 3 and 4) could be coincident with the surface ruptures of historical earthquakes. The Quaternary alluvial sediments from *La Torrecilla* Creek cover the fault rock, but when they appear on the lowest parts of the fault rock (domains 3, 4 and 5), we found faults that offset them (red fault in Figure 2). In T4, Martinez-Díaz et al. [29] showed a surface rupture that offsets an Arabic archaeological remain at this point (see Supplementary Material (available here)). This rupture was related to the 1674 catastrophic event occurred in Lorca (Murcia). Moreover, domain 1 is covered by undeformed old Quaternary hardened glacis deposits supporting that this sector of the fault zone is not utilized by recent ruptures, at least at shallow levels. This may be pointing that the sense of growing of the shear zone vary from the hanging wall, where steady deformation occurs (domain 1), towards the footwall of the shear, where historical earthquakes ruptures are being recorded (Figure 10).

5.2. On the Architecture of the Fault Zone and Spatial Distribution of Its Lithologies. Summarizing, as we see above, the architecture of the AMF is composed of 10 to 30 meters wide fault core with a narrow damage zone in its upper limit (less than 5 meters wide) and a wide (more than 70 meters wide), highly deformed and heterogenous damage zone towards its lower limit, that is covered by recent sediments that prevent seeing it. All the observations point to an asymmetric slip (strain) distribution across the fault zone; accordingly, this fault zone is far from those conceptual models of symmetric strain distribution of Chester and Logan [12] or Faulkner et al. [7] (Figure 11). These models consist of three primary components in a shear zone: the hosting rock, the damage zone, and the fault core (where almost all the strain is accommodated Chester et al., 1993; [13, 76]). Chester and Logan [12] model consist of a fault core in the middle of the shear zone where almost all the strain is concentrated, decreasing towards both sides equally. The Faulkner et al.'s [7] model (based on Carboneras Fault, see Figure 1) has a more complex distribution of the strain and anastomosed fault core appear, but strain is still distributed symmetrically (Figure 11). Faulkner et al. [7] explained the differences into anastomosed versus single straight core of a fault rock based on compositional features; Chester and Logan's [12] model could be assumed for quartzofeldesphatic hosting rocks, while Faulkner's et al. [7] model is based on philosilicate-rich hosting rocks that bound lenses of variably fractured protolith. The mechanical properties of philosilicate rich fault rocks may explain these features, because strain hardening is a common process in these rocks while weakening is more common in quartzofeldspathic rocks [23, 77, 78]. AMF hosting rocks are very similar to the Carboneras Fault rocks, and the mechanical features of them may explain the anastomosing distribution of the strain, but not its asymmetric distribution.

As explained above from domain 3 Subsidiary Slip Zones appear, whereas in domains 1 and 2 deformation is homogeneously distributed. In domains 3 and 4, SSZs correspond to anastomosed 2 to 10 cm wide shear planes that seem to have accommodated more deformation than the bounding fault rock (that still presents comminution and shearing indicators). However, when the strain decreases and the hosting rock has not been overprinted by the new tectonic fabric, the SSZs still appear. Domain 5 is lithologically almost homogeneous (composed mostly of Blue/Gray phyllites, with some lateral intercalation of Malaguide Complex and Miocene rocks), and the SSZs are anastomosed shear zones bounding blocks with low deformation grade; thereby, we think that the SSZs in this case could be connected with the strain distribution at depth being closer to the Faulkner's et al. [7] model.

For all these reasons, here, we propose a hybrid and asymmetric model based on both Chester and Logan [12] and Faullkner et al. [7] models and more specifically on Lin and Yamashita [79] that showed that there are spatial variations of the fault core location along strike and that the strain

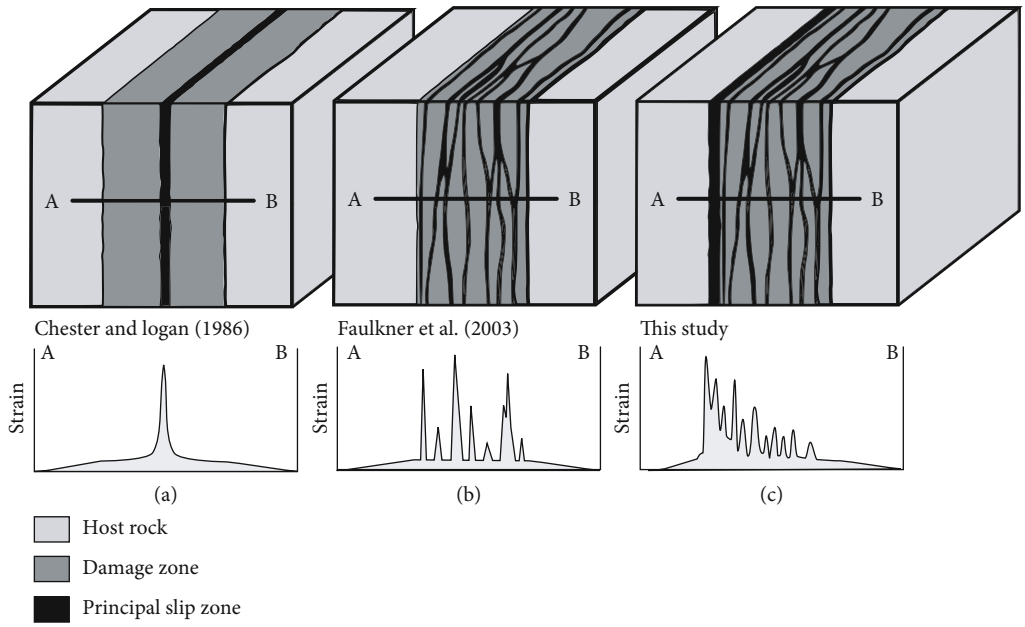

Figure 11: Conceptual models of a fault zone architecture. (a) Chester and Logan [12] model. (b) Faulkner et al. [7] model. (c) This study, asymmetric hybrid model.

distribution could be highly asymmetric even in a strike-slip fault. Here, the strain starts abruptly in one of the sides of the shear zone where the strain is the highest (fault core), and there is almost no damage zone in the transition between the core and the hosting rock. The strain tends to decrease towards the other side and anastomosed shear planes appear, which accommodate more deformation than the hosting rock. Domains 1 and 2 are the fault core; from domain 3, the decreasing trend of the strain starts. From this point, an architecture dominated by an alternation of SSZs and less deformed blocks appear, and the strain differences between SSZs and damage zone are increasing towards the end of the shear zone (Figures 10 and 11).

5.3. On the Asymmetry of the Shear Zone. It is intriguing that, in a shear zone with more than 10 km accumulated slip [20], the damage zone is located at only one side of the core, which is in contact with an almost no deformed hanging wall to its opposite side. Inclined shear zones display asymmetry of the damage zone (e.g., [79–82]). Numerical models showing mechanical asymmetries in both normal and reverse faults done by Ma (2009) together with several observations in natural damage zones for example Heermace et al. [83], Yeh et al. [84] at Chelungpu Fault or Li et al. [85] at Yingxiu-Beichuan Fault Zone showed that, contrary to the results of this study, the wider damage zones are located in the hanging wall of the fault zones. Seems thereby that the AMF could be an exception where the damage zone is located mostly in the footwall. This strain heterogeneity and the asymmetric distribution of the slip could be explained by several reasons: mechanical heterogeneities related to sedimentary and basement material juxtaposition; mechanical anisotropies related to fault propagation and growth (i.e., splay formation during reverse faulting); intrinsic kinematic features of an inclined shear zone; or a combination of two or more processes.

The mechanical contrasts in shear zones could arise in a heterogeneous strain distribution [86–89]. The basement rocks of Alpujarride and Malaguide Complexes together with sedimentary rocks from the Lorca and Guadalentin basins may arise in a complex distribution of the slip (at least at surface). The phyllosillicate rich protoliths may promote strain hardening and thereby the widening of the shear zone, while the sedimentary rocks are involved in the shear zone introducing heterogeneties. This mixture of textures could incorporate roughness in the lower part of the shear zone, and the asperity removal and comminution place the slip in the boundaries of sedimentary blocks, resulting in the slip heterogeneities found in domains 3 and 4. But this explanation does not completely satisfy the observations in domain 5 which is composed of basement rocks and located at the bottom of the shear zone. Another possibility in order to explain the strong asymmetry in the shear zone could be related to the hanging wall imbrication and splay formation during shearing towards the footwall where recent slip events are recorded. The kinematic evolution of a fold-and-thrust belt implies tilting of the thrusts until reach a critical dip angle enabling the formation of new thrusts towards the foreland (e.g., [90]). A similar process with different critical dip angles could had promoted the appearance of new faults towards the footwall of the shear zone involving new protolith lenses and promoting the observed asymmetry.

The decreasing trend in strain intensity towards the footwall of the shear zone could be also explained as a part of the deformation mechanism in an inclined transpressive triclinic shear zone. Nabavi et al. [91] used finite element to model an inclined shear zone similar to the kinematic model of Inclined Transpression with Oblique Extrusion ([92], that has satisfactorily explained the strain distribution in the AMF, [25]). With a set-up where two reverse faults (dipping 70°) are bounding a shear zone, Nabavi et al. [91] revealed

that the velocity vectors within the shear zone gradually decrease towards the footwall. This model explains that the accommodated slip close to the hanging wall is the higher, and also, it could explain why steady deformation is located in domain 1, but it does not explain why the surface ruptures of historical earthquakes are located towards the footwall, but this fact, together with splay formation, would explain both the asymmetry and the location of the last increments of strain in the footwall of the fault.

6. Conclusions

The study of tectonic fabric at both microscale and outcrop-scale of the fault rocks of the Alhama de Murcia Fault reveals that:

(1) Predominant deformation mechanisms are brecciation, cataclasis, frictional sliding, and cataclastic flow, but several optical microscopic observations reveal that frictional melting and intracrystalline deformation could be also deformation mechanisms within this shear zone

(2) The strain distribution in this shear zone is highly asymmetric; it decreases from hanging wall to the footwall. Steady homogeneous deformation was found in domains 1 and maybe 2, areas closest to the hanging wall where comminution made a matrix percentage higher than 90% of the fault rock. As deformation increased, it involved sedimentary rocks of Lorca basin in domains with a highly heterogeneous strain distribution. In the lowermost domain, strain is located in anastomosed shear bands (here classified as Subsidiary Slip Zones) which are spatially related with a surface seismic rupture of the 1674 destructive earthquake

(3) The mechanical heterogeneities of the different protoliths within domain 3 may had conditioned the heterogeneity in the slip distribution and the competency contrast favors slip in the block boundaries. This fact is visible both at outcrop scale and microscope scale, where we found protolith blocks with almost no deformation (apart from some microfractures) while out of them foliated gouges appear

(4) The inclined transpression models together with and splay formation during reverse faulting are the preferred hypothesis to explain the strain asymmetry of the shear zone, but we cannot discard mechanical heterogeneities caused by juxtaposition of sedimentary and basement rocks as an other plausible explanation

Data Availability

Data are available by contacting with corresponding author and in supplementary material.

Conflicts of Interest

The authors declare that they have no conflicts of interest.

Acknowledgments

This research was supported by the project "QUAKESTEP" (CGL2017–83931-C3-1-P) founded by the Spanish Ministry of Science, Innovation and Universities. We thank Marián Barajas López (Complutense University of Madrid) for thin section preparation. We thank José L. Sanchez Roldán, Yolanda de Pro, and Juan Miguel Insúa Arrévalo (Complutense University of Madrid) for their support during sampling and Alejandra Staller (Polytechnic University of Madrid) for drone image acquisition. We thank Associate Editor Andrea Billi and the reviewer Jack Williams for their constructive comments done on the original version of this article.

Supplementary Materials

Supplementary material consists of photo logs of the excavated trenches for sampling, aerial photograph of the study area, and lower hemisphere plots of planes and lines within the shear zone. *(Supplementary Materials)*

References

[1] R. E. Holdsworth, E. W. E. van Diggelen, C. J. Spiers, J. H. P. de Bresser, R. J. Walker, and L. Bowen, "Fault rocks from the SAFOD core samples: implications for weakening at shallow depths along the San Andreas Fault, California," *Journal of Structural Geology*, vol. 33, no. 2, pp. 132–144, 2011.

[2] H. Kanamori and E. Brodsky, "The physics of earthquakes," *Reports on Progress in Physics*, vol. 67, no. 8, pp. 1429–1496, 2004.

[3] C. H. Scholz, *The Mechanics of Earthquakes and Faulting*, Cambridge University Press, Cambridge, 2002.

[4] R. Sutherland, J. Townend, V. Toy et al., "Extreme hydrothermal conditions at an active plate-bounding fault," *Nature*, vol. 546, no. 7656, pp. 137–140, 2017.

[5] M. D. Zoback, S. H. Hickman, and B. Ellsworth, "Scientific drilling into the San Andreas fault zone," *Eos: Transactions of the American Geophysical Union*, vol. 91, no. 22, pp. 197–199, 2010.

[6] N. Barth, C. Boulton, B. Carpenter, G. Batt, and V. Toy, "Slip localization on the southern Alpine Fault, New Zealand," *Tectonics*, vol. 32, no. 3, pp. 620–640, 2013.

[7] D. R. Faulkner, A. C. Lewis, and E. H. Rutter, "On the internal structure and mechanics of large strike-slip fault zones: field observations of the Carboneras fault in southeastern Spain," *Tectonophysics*, vol. 367, no. 3-4, pp. 235–251, 2003.

[8] D. R. Faulkner, T. M. Mitchell, E. H. Rutter, and J. Cembrano, "On the structure and mechanical properties of large strike-slip faults," in *Geological Society, London, Special Publications*, C. A. J. Wibberley, W. Kurz, J. Imber, R. E. Holdsworth, and C. Collettini, Eds., vol. 299, no. 1pp. 139–150, Geological Society of London Special Publication, 2008.

[9] V. Toy, R. J. Norris, D. J. Prior, M. Walrond, and A. F. Cooper, "How do lineations reflect the strain history of transpressive shear zones? The example of the active Alpine Fault zone, New Zealand," *Journal of Structural Geology*, vol. 50, pp. 187–198, 2013.

[10] V. Toy, C.-J. Boulton, R. Sutherland et al., "Fault rock lithologies and architecture of the Central Alpine fault, New Zealand,

revealed by DFDP-1 drilling," *Lithosphere*, vol. 7, no. 2, pp. 155–173, 2015.

[11] J. Caine, J. Evans, and C. Forster, "Fault zone architecture and permeability structure," *Geology*, vol. 24, no. 11, pp. 1025–1028, 1996.

[12] F. M. Chester and J. M. Logan, "Implications for mechanical properties of brittle faults from observations of the Punchbowl fault zone, California," *Pure and Applied Geophysics*, vol. 124, no. 1-2, pp. 79–106, 1986.

[13] R. Biegel and C. Sammis, "Relating fault mechanics to fault zone structure," *Advances in Geophysics*, vol. 47, pp. 65–111, 2004.

[14] C. Janssen, R. Wirth, H.-R. Wenk et al., "Faulting processes in active faults - evidences from TCDP and SAFOD drill core samples," *Journal of Structural Geology*, vol. 65, pp. 100–116, 2014.

[15] R. Sibson, "Thickness of the seismic slip zone," *Bulletin of the Seismological Society of America*, vol. 93, no. 3, pp. 1169–1178, 2003.

[16] J. García-Mayordomo, J. M. Insua-Arévalo, J. J. Martínez-Díaz et al., "The quaternary Active faults database of Iberia (QAFI v.2.0)," *Journal of Iberian Geology*, vol. 38, no. 1, pp. 285–302, 2012.

[17] J. Á. López-Comino, F. Mancilla, J. Morales, and D. Stich, "Rupture directivity of the 2011, Mw 5.2 Lorca earthquake (Spain)," *Geophysical Research Letters*, vol. 39, no. 3, article L03301, 2012.

[18] E. Masana, J. J. Martínez-Díaz, J. L. Hernández-Enrile, and P. Santanach, "The Alhama de Murcia fault (SE Spain), a seismogenic fault in a diffuse plate boundary: Seismotectonic implications for the Ibero-Magrebian region," *Journal of Geophysical Research*, vol. 109, no. B1, pp. 1–17, 2004.

[19] E. Rodríguez-Escudero, J. J. Martínez-Díaz, J. A. Álvarez-Gómez, J. M. Insua-Arévalo, and R. Capote del Villar, "Tectonic setting of the recent damaging seismic series in the Southeastern Betic Cordillera, Spain," *Bulletin of Earthquake Engineering*, vol. 12, no. 5, pp. 1831–1854, 2014.

[20] E. H. Rutter, R. H. Maddock, S. H. Hall, and S. H. White, "Comparative microstructures of natural and experimentally produced clay-bearing fault gouges," *pure and applied geophysics*, vol. 124, no. 1-2, pp. 3–30, 1986.

[21] S. H. Hall, *Post-alpine tectonic evolution of SE Spain and the structure of fault gouge [Ph.D. thesis]*, University of London, London, 1983.

[22] E. H. Rutter, D. R. Faulkner, and R. Burgess, "Structure and geological history of the Carboneras Fault Zone, SE Spain: part of a stretching transform fault system," *Journal of Structural Geology*, vol. 45, pp. 68–86, 2012.

[23] A. R. Niemeijer and R. L. Vissers, "Earthquake rupture propagation inferred from the spatial distribution of fault rock frictional properties," *Earth and Planetary Science Letters*, vol. 396, pp. 154–164, 2014.

[24] E. Rodríguez-Escudero, J. J. Martínez-Díaz, J. L. Giner-Robles, M. Tsige, and J. Cuevas-Rodríguez, "Pulverized quartz clasts in gouge of the Alhama de Murcia fault (Spain): evidence for coseismic clast pulverization in a matrix deformed by frictional sliding," *Geology*, vol. 48, no. 3, pp. 283–287, 2020.

[25] J. Alonso-Henar, C. Fernánadez, and J. J. Martínez-Díaz, "Application of the analytic model of general triclinic transpression with oblique extrusion to an active deformation zone: the Alhama de Murcia Fault (SE Iberian Peninsula)," *Journal of Structural Geology*, vol. 130, article 103924, 2020.

[26] M. Ferrater, M. Ortuño, E. Masana et al., "Refining seismic parameters in low seismicity areas by 3D trenching: the Alhama de Murcia fault, SE Iberia," *Tectonophysics*, vol. 680, pp. 122–128, 2016.

[27] P. Herrero-Barbero, J. A. Álvarez-Gómez, J. J. Martínez-Díaz, and J. Klimowitz, "Neogene basin inversion and recent slip rate distribution of the northern termination of the Alhama de Murcia Fault (Eastern Betic Shear Zone, SE Spain)," *Tectonics*, vol. 39, no. 7, 2020.

[28] J. J. Martínez-Díaz, E. Masana, J. L. Hernández-Enrile, and P. Santanach, "Effects of the paleoseismic activity of an oblique slip fault on the morphology and sedimentology of an alluvial fan (Alhama de Murcia fault, Betic Cordillera-Spain)," *Annals of Geophysics*, vol. 46-5, pp. 775–793, 2003.

[29] J. J. Martínez-Díaz, J. Alonso-Henar, J. M. Insua-Arévalo et al., "Geological evidences of surface rupture related to a seventeenth century destructive earthquake in Betic Cordillera (SE Spain): constraining the seismic hazard of the Alhama de Murcia fault," *Journal of Iberian Geology*, vol. 45, no. 1, pp. 73–86, 2019.

[30] M. Ortuno, E. Masana, E. Garcia-Melendez et al., "An exceptionally long paleoseismic record of a slow-moving fault: the Alhama de Murcia fault (Eastern Betic Shear Zone, Spain)," *Geological Society of America Bulletin*, vol. 124, no. 9–10, pp. 1474–1494, 2012.

[31] J. C. Bousquet and C. Montenat, "Presence de décrochements NE-SW plioquatemaires dans les Cordilleres Bétiques Orientales (Espagne)," in *Extension et signification général*, vol. 278, pp. 2617–2620, Comptes Rendus de l'Académie des Sciences Paris, 1974.

[32] F. D. de Larouzière, J. J. Bolze, P. Bordet, J. Hernandez, C. Montenat, and P. Ott d'Estevou, "The Betic segment of the lithospheric trans-Alboran shear zone during the late Miocene," *Tectonophysics*, vol. 152, no. 1-2, pp. 41–52, 1988.

[33] P. Alfaro, R. Bartolomé, M. J. Borque et al., "The Bajo Segura Fault Zone: active blind thrusting in the Eastern Betic Cordillera (SE Spain)," *Journal of Iberian Geology*, vol. 38, no. 1, pp. 271–284, 2012.

[34] J. W. Bell, F. Amelung, and G. C. P. King, "Preliminary late quaternary slip history of the Carboneras fault, Southeastern Spain," *Journal of Geodynamics*, vol. 24, no. 1–4, pp. 51–66, 1997.

[35] R. Martín-Banda, J. García-Mayordomo, J. M. Insua-Arévalo et al., "New insights on the seismogenic potential of the Eastern Betic Shear Zone (SE Iberia): quaternary activity and paleoseismicity of the SW segment of the Carrascoy Fault Zone," *Tectonics*, vol. 35, no. 1, pp. 55–75, 2016.

[36] R. Martín-Banda, J. M. Insua-Arévalo, and J. García-Mayordomo, "Slip rate variation during the last ~210 ka on a slow fault in a transpressive regime: the Carrascoy Fault (Eastern Betic Shear Zone, SE Spain)," *Frontiers in Earth Science*, vol. 8, article 599608, 2021.

[37] P. G. Silva, J. L. Goy, L. Somoza, C. Zazo, and T. Bardaji, "Landscape response to strike-slip faulting linked to collisional settings: quaternary tectonics and basin formation in the Eastern Betics, southeastern Spain," *Tectonophysics*, vol. 224, no. 4, pp. 289–303, 1993.

[38] M. J. Borque, A. Sánchez-Alzola, I. Martin-Rojas et al., "How much Nubia-Eurasia convergence is accommodated by the NE end of the Eastern Betic Shear Zone (SE Spain)? Constraints from GPS velocities," *Tectonics*, vol. 38, no. 5, pp. 1824–1839, 2019.

[39] A. Echeverria, G. Khazaradze, E. Asensio, J. Gárate, J. M. Dávila, and E. Suriñach, "Crustal deformation in eastern Betics from CuaTeNeo GPS network," *Tectonophysics*, vol. 608, pp. 600–612, 2013.

[40] J. J. Martínez-Díaz, M. Bejar-Pizarro, J. A. Álvarez-Gómez et al., "Tectonic and seismic implications of an intersegment rupture: The damaging May 11th 2011 Mw 5.2 Lorca, Spain, earthquake," *Tectonophysics*, vol. 546-547, pp. 28–37, 2012.

[41] M. Ferrater, M. Ortuño, E. Masana et al., "Lateral slip rate of Alhama de Murcia fault (SE Iberian Peninsula) based on a morphotectonic analysis: comparison with paleoseismological data," *Quaternary International*, vol. 451, pp. 87–100, 2017.

[42] J. J. Martínez-Díaz, E. Masana, and M. Ortuño, "Active tectonics of the Alhama de Murcia fault, Betic Cordillera, Spain," *Journal of Iberian Geology*, vol. 38, no. 1, pp. 253–270, 2012.

[43] E. Rodríguez-Escudero, *Implicaciones de la estructura interna de una zona de falla activa en la genesis de terremotos [PhD Thesis]*, Universidad Autonomoa de Madrid, 2017.

[44] M. T. Gómez-Pugnaire, D. Rubatto, J. M. Fernández-Soler et al., "Late Variscan magmatism in the Nevado-Filabride Complex: U-Pb geochronologic evidence for the pre-Mesozoic nature of the deepest Betic complex (SE Spain)," *Lithos*, vol. 146-147, pp. 93–111, 2012.

[45] J. C. Balanyá and V. García-Dueñas, *Les directions structurales dans le Domaine d'Alborán de part et d'autre du Détroit de Gibraltar*, vol. 304 of Série II, , no. 15, 1987Comptes Rendus de l'Académie des Sciences de Paris, 1987.

[46] R. Armijo, *La zona des failles Lorca-Totana (Cordilleres Betiques, Espagne). Etude tectonique et neotectonique [Ph.D. Thesis]*, University. Paris VII, 1977.

[47] J. Rodríguez-Fernández, A. Azor, and J. Miguel Azañón, "The Betic intramontane basins (SE Spain): stratigraphy, subsidence, and tectonic history," in *Tectonics of Sedimentary Basins: Recent Advances*, C. Busby and A. Azor, Eds., vol. 23, pp. 461–479, Blackwell Publishing Ltd, Chichester, UK, 2012.

[48] A. Acosta, *Estudio de los fenómenos de fusión cortical y generación de granitoides asociados a las peridotitas de Ronda. [PhD Thesis]*, Universidad de Granada, 1997.

[49] G. Booth-Rea, J. M. Azañón, and V. García-Dueñas, "Extensional tectonics in the northeastern Betics (SE Spain): case study of extension in a multilayered upper crust with contrasting rheologies," *Journal of Structural Geology*, vol. 26, no. 11, pp. 2039–2058, 2004.

[50] L. Lonergan and J. Platt, "The Malaguide-Alpujarride boundary: a major extensional contact in the internal zone of the eastern Betic Cordillera, SE Spain," *Journal of Structural Geology*, vol. 17, no. 12, pp. 1655–1671, 1995.

[51] L. Sánchez-Rodríguez and D. Gebauer, "Mesozoic formation of pyroxenites and gabbros in the Ronda area (southern Spain), followed by Early Miocene subduction metamorphism and emplacement into the middle crust: U-Pb sensitive high-resolution ion microprobe dating of zircon," *Tectonophysics*, vol. 316, no. 1-2, pp. 19–44, 2000.

[52] H. P. Zeck and M. J. Whitehouse, "Hercynian, Pan-African, Proterozoic and Archean ion-microprobe zircon ages for a Betic-RIF core complex, Alpine Belt, W Mediterranean-consequences for Its *P-T-T* Path," *Contributions to Mineralogy and Petrology*, vol. 134, no. 2-3, pp. 134–149, 1999.

[53] F. Álvarez, *La tectónica de la Zona Bética en la región de Águilas [PhD Thesis]*, University of Salamanca, 1987, Unpublished Doctoral thesis.

[54] W. C. P. De Vries and K. B. Zwaan, "Alpujárride succesion in the central Sierra de las Estancias, province of Almería, SE Spain," *Proceedings Of The Koninklijke Nederlandse Akademie Van Wetenschappen Series B-Physical Sciences*, vol. 70, no. 4, pp. 443–453, 1967.

[55] H. Kozur, W. Kampschuur, C. W. Mulder-Blanken, and O. J. Simon, "Contribution to the Triassic ostracode faunas of the Betic Zone (southern Spain)," *Scripta Geologica*, vol. 23, pp. 1–56, 1974.

[56] H. Kozur, C. W. H. Mulder-Blanken, and O. J. Simon, "On the triassic of the betic cordilleras (southern Spain), with special emphasis on holothurian selerites," *Stratigraphy and Paleontology*, vol. 88, pp. 83–110, 1985.

[57] I. Abad, F. Nieto, D. R. Peacor, and N. Velilla, "Prograde and retrograde diagenetic and metamorphic evolution in metapelitic rocks of Sierra Espuña (Spain)," *Clay Minerals*, vol. 38, no. 1, pp. 1–23, 2003.

[58] L. Lonergan, *Structural Evolution of the Sierra Espuña, Betic Cordillera, SE Spain [PhD. Thesis]*, Oxford University, 1991.

[59] F. Nieto, N. Velilla, D. R. Peacor, and M. O. Huertas, "Regional retrograde alteration of sub-greenschist facies chlorite to smectite," *Contributions to Mineralogy and Petrology*, vol. 115, no. 3, pp. 243–252, 1994.

[60] G. Booth-Rea, P. G. Silva, and J. A. Santos-García, *Cartografía Geológica y Memoria de Puerto Lumbreras*, vol. 975Instituto Geológico y Minero de España, Edición Digital del Mapa Geológico de España, escala 1: 50000, Hoja núm edition, 2008.

[61] B. M. L. Meijninger, "Late-orogenic extension and strike-slip deformation in the neogene of southeastern Spain," *Geologica Ultraiectina*, vol. 269, 2006.

[62] A. Estévez, J. Rodríguez-Fernández, C. Sanz de Galdeano, and J. A. Vera, "Evidencia de una fase compresiva de edad Tortoniense en el sector central de las Cordilleras béticas," *Estudios Geológicos*, vol. 30, pp. 55–60, 1982.

[63] C. H. Montenat, P. H. Ott D'Estevou, and G. Coppier, *Les bassins neogenes entre Alicante et Cartagena*, vol. 12-13, Documents et travaux de l'Institut géologique Albert de Lapparent, 1990.

[64] P. Silva, *Evolución geodinámica de la Depresión del Guadalentín desde el Mioceno Superior hasta la actualidad: neotectónica y geomorfología [PhD. Thesis]*, Universidad Complutense de Madrid, 1994.

[65] J. M. Rouchy, C. Taberner, M. M. Blanc-Valleron et al., "Sedimentary and diagenetic markers of the restriction in a marine basin: the Lorca Basin (SE Spain) during the Messinian," *Sedimentary Geology*, vol. 121, no. 1-2, pp. 23–55, 1998.

[66] P. G. Silva, T. Bardají, M. Calmel-Avila, J. L. Goy, and C. Zazo, "Transition from alluvial to fluvial systems in the Guadalentin Depression (SE Spain) during the Holocene: Lorca Fan _versus_ Guadalent in River," *Geomorphology*, vol. 100, no. 1–2, pp. 140–153, 2008.

[67] J. J. Martínez-Díaz, M. J. Jurado, J. Crespo, and R. Capote, "FAM-1 borehole: first results from the scientific drilling of the Alhama de Murcia Fault, Betic cordillera, Spain," *Geo Temas*, vol. 16, no. 2, pp. 579–582, 2016.

[68] M. Díaz-Azpiroz, C. Fernandez, and D. M. Czeck, "Are we studying deformed rocks in the right sections? Best practices in the kinematic analysis of 3D deformation zones," *Journal of Structural Geology*, vol. 125, pp. 218–225, 2019.

[69] N. H. Woodcock and K. Mort, "Classification of fault breccias and related fault rocks," *Geological Magazine*, vol. 145, no. 3, pp. 435–440, 2008.

[70] J. Schindelin, I. Arganda-Carreras, E. Frise et al., "Fiji: an open-source platform for biological-image analysis," *Nature methods*, vol. 9, no. 7, pp. 676–682, 2012.

[71] N. K. Tovey and W. K. Wong, "The preparation of soils and other geological material for the SEM International symposium on soil structure," *Gothenburg*, vol. 1973, pp. 59–69, 1973.

[72] A. M. Killick, "Fault rock classification: an aid to structural interpretation in mine and exploration geology," *South African Journal of Geology*, vol. 106, no. 4, pp. 395–402, 2003.

[73] R. Sibson, "Fault rocks and fault mechanisms," *Journal of the Geological Society of London*, vol. 133, no. 3, pp. 191–213, 1977.

[74] T. G. Blenkinshop, "Cataclasis and processes of size reduction," *pure and applied geophysics*, vol. 136, no. 1, pp. 59–86, 1991.

[75] L. B. Goodwin and B. Tikoff, "Competency contrast, kinematics, and the development of foliations and lineations in the crust," *Journal of Structural Geology*, vol. 24, no. 6-7, pp. 1065–1085, 2002.

[76] D. Faulkner, C. A. L. Jackson, R. Lunn et al., "A review of recent developments concerning the structure, mechanics and fluid flow properties of fault zones," *Journal of Structural Geology*, vol. 32, no. 11, pp. 1557–1575, 2010.

[77] J. H. Dieterich, "Modeling of rock friction: 1. Experimental results and constitutive equations," *Journal of Geophysical Research: Solid Earth*, vol. 84, no. B5, pp. 2161–2168, 1979.

[78] J. M. Fletcher, O. J. Teran, T. K. Rockwell et al., "An analysis of the factors that control fault zone architecture and the importance of fault orientation relative to regional stress," *GSA Bulletin*, vol. 132, no. 9-10, pp. 2084–2104, 2020.

[79] A. Lin and K. Yamashita, "Spatial variations in damage zone width along strike-slip faults: an example from active faults in southwest Japan," *Journal of Structural Geology*, vol. 57, pp. 1–15, 2013.

[80] M. Antonellini and A. Aydin, "Effect of faulting on fluid flow on porous sandstones: petrophysical properties," *American Association of Petroleum Geologists Bulletin*, vol. 78, no. 3, pp. 355–377, 1994.

[81] S. S. Berg and T. Skar, "Controls on damage zone asymmetry of a normal fault zone: outcrop analyses of a segment of the Moab fault, SE Utah," *Journal of Structural Geology*, vol. 27, no. 10, pp. 1803–1822, 2005.

[82] G. Mitra and Z. Ismat, "Microfracturing associated with reactivated fault zones and shear zones: what can it tell us about deformation history?," in *The Nature and Tectonic Significance of Fault Zone Weakening Geological Society*, R. E. Holdsworth, R. A. Strachan, J. F. Magloughlin, and R. J. Knipe, Eds., vol. 186, pp. 113–140, Special Publications, London, 2001.

[83] R. Heermance, Z. K. Shipton, and J. P. Evans, "Fault structure control on fault slip and ground motion during the 1999 rupture of the Chelungpu fault, Taiwan," *Bulletin of the Seismological Society of America*, vol. 93, no. 3, pp. 1034–1050, 2003.

[84] E. C. Yeh, H. Sone, T. Nakaya et al., "Core description and characteristics of fault zones from Hole-A of the Taiwan Chelungpu-Fault Drilling Project," *TAO: Terrestrial, Atmospheric and Oceanic Sciences*, vol. 18, no. 2, p. 327, 2007.

[85] H. Li, H. Wang, Z. Xu et al., "Characteristics of the fault-related rocks, fault zones and the principal slip zone in the Wenchuan Earthquake Fault Scientific Drilling Project Hole-1 (WFSD-1)," *Tectonophysics*, vol. 584, pp. 23–42, 2013.

[86] H. Fossen and G. C. G. Cavalcante, "Shear zones - a review," *Earth-Science Reviews*, vol. 171, pp. 434–455, 2017.

[87] R. Norris and V. Toy, "Continental transforms: a view from the Alpine Fault," *Journal of Structural Geology*, vol. 64, pp. 3–31, 2014.

[88] C. Schrank, M. Handy, and F. Fusseis, "Multiscaling of shear zones and the evolution of the brittle-to-viscous transition in continental crust," *Journal of Geophysical Research*, vol. 113, no. B1, 2008.

[89] J. M. Scott, A. Auer, J. R. Muhling et al., "New P–T and U–Pb constraints on Alpine Schist metamorphism in south Westland, New Zealand," *Journal of Geophysical Research*, vol. 58, no. 4, pp. 385–397, 1983.

[90] J. Poblet and R. J. Lisle, "Kinematic evolution and structural styles of fold-and-thrust belts," *Geological Society, London, Special Publications*, vol. 349, no. 1, pp. 1–24, 2011.

[91] S. T. Nabavi, S. A. Alavi, M. Díaz-Azpiroz et al., "Deformation mechanics in inclined, brittle-ductile transpression zones: insights from 3D finite element modelling," *Journal of Structural Geology*, vol. 137, article 104082, 2020.

[92] C. Fernández and M. Díaz-Azpiroz, "Triclinic transpression zones with inclined extrusion," *Journal of Structural Geology*, vol. 31, no. 10, pp. 1255–1269, 2009.

[93] E. Brodsky, J. J. Gilchrist, A. Sagy, and C. Collettini, "Faults smooth gradually as a function of slip," *Earth and Planetary Science Letters*, vol. 302, no. 1-2, pp. 185–193, 2011.

[94] T. T. Cladouhos, "Shape preferred orientations of survivor grains in fault gouge," *Journal of Structural Geology*, vol. 21, no. 4, pp. 419–436, 1999.

[95] I. Geológicoy, M. de España, and IGME, "QAFI v.3: quaternary active faults database of Iberia," 2015, http://info.igme.es/QAFI/.

[96] j. V. A. Keller, s. H. Hall, c. J. Dart, and k. R. Mcclay, "The geometry and evolution of a transpressional strike-slip system: the Carboneras fault, SE Spain," *Journal of the Geological Society of London*, vol. 152, no. 2, pp. 339–351, 1995.

[97] J. J. Martínez-Díaz, E. Masana, J. L. Hernández-Enrile, and P. Santanach, "Evidence for coseismic events of recurrent prehistoric deformation along the Alhama de Murcia fault, southeastern Spain," *Acta Geologica Hispanica*, vol. 36, no. 3–4, pp. 315–327, 2001.

[98] J. M. Martínez-Martínez and J. M. Azañón, "Mode of extensional tectonics in the southeastern Betics (SE Spain): implications for the tectonic evolution of the peri-Alborán orogenic system," *Tectonics*, vol. 16, no. 2, pp. 205–225, 1997.

[99] B. Schuck, A. M. Schleicher, C. Janssen, V. Toy, and G. Dresen, "Fault zone architecture of a large plate-bounding strike-slip fault: a case study from the Alpine Fault, New Zealand," *Solid Earth*, vol. 11, no. 1, pp. 95–124, 2020.